A SUBCRITICAL, HELIUM-COOLED FAST REACTOR FOR THE TRANSMUTATION OF SPENT NUCLEAR FUEL

RADIOACTIVE WASTE MANAGEMENT AND DISPOSAL

KEYWORDS: *transmutation, fast reactor, fusion neutron source*

W. M. STACEY,* Z. ABBASI, C. J. BOYD, A. H. BRIDGES, E. A. BURGETT, M. W. CYMBOR, S. W. FOWLER, A. T. JONES, R. S. KELM, B. J. KERN, D. B. LASSITER, J. A. MADDOX, W. B. MURPHY, H. PARK, J. M. POUNDERS, and J. R. PRESTON

Georgia Institute of Technology, Nuclear and Radiological Engineering Program
Atlanta, Georgia 30332-0425

Received August 16, 2005
Accepted for Publication February 9, 2006

A design concept and supporting analysis are presented for a He-cooled fast reactor for the transmutation of spent nuclear fuel. Coated transuranic (TRU) fuel particles in a SiC matrix are used. The reactor operates subcritical ($k \leq 0.95$), with a tokamak D-T fusion neutron source, to achieve >90% TRU burnup in repeated five-batch fuel cycles, fissions 1.1 tonnes/full-power year, and produces 700 MW(electric) net electrical power. The reactor design is based on nuclear, fuels, materials, and separations technologies being developed in the Generation-IV, Next Generation Nuclear Plant, and Advanced Fuel Cycle Initiative programs and similar international programs, and the fusion neutron source is based on the physics and technology supporting the ITER design.

I. INTRODUCTION

Advanced reactor concepts with fuel cycles that better utilize fuel resources and reduce high-level waste repository requirements are being studied intensively in the U.S. Generation-IV Nuclear Energy Systems Initiative[1] (GEN-IV) and the Advanced Fuel Cycle Initiative[2] and in related studies worldwide. In parallel, as part of the Next Generation Nuclear Plant (NGNP) project,[3] a research and development program is under way on the further development of coated fuel particle technology with an objective of achieving extremely high burnup without fission product release.

*E-mail: weston.stacey@nre.gatech.edu

The further development of coated fuel particle technology has stimulated the examination of "deep-burn" transmutation reactors that could destroy up to 90% or more of the transuranic (TRU) waste remaining in the spent nuclear fuel (SNF) from light water reactors (LWRs) in thermal[4] and fast[5] gas-cooled reactors. In both cases, 90% burnup was achieved by subcritical operation with an accelerator[4] or fusion[5] neutron source.

Our purpose in this paper is to extend our previous study[5] of a subcritical, He-cooled fast reactor with coated TRU fuel particles and a tokamak D-T fusion neutron source, denoted the Gas Cooled Fast Transmutation Reactor (GCFTR). As in the previous study, the design objectives were (a) to achieve ≥90% TRU burnup and (b) to use a physics and technology design basis for both the reactor and the fusion neutron source that either exists or is being developed in ongoing research and development programs so that a 2040 deployment timescale is feasible.

The paper is organized as follows: An overview of the new GCFTR-2 design concept, the materials and major parameters of the principal systems, the performance parameters, and the radiation damage lifetimes of the principal components are given in Sec. II. The aqueous reprocessing system for separating the TRU from the SNF, the coated TRU fuel particle and its fabrication system, an analysis of the coated TRU fuel particle lifetime against fission product gas buildup and corrosion, and the study of fuel element configuration leading to the choice of the coated particle embedded in a SiC matrix fuel pin configuration are presented in Sec. III. The nuclear analysis of the fuel configuration options, the fuel enrichment, the tritium production, reactivity coefficients, decay heat, and the design of the shield to protect the superconducting magnets from radiation damage and nuclear heating are described in Sec. IV. The nuclear fuel

cycle analysis and the transmutation performance are presented in Sec. V. The plasma performance, magnet and divertor systems, and the tritium production requirements of the tokamak D-T fusion neutron source are discussed in Sec. VI. Thermal analyses of the nominal core operation for various options for the fuel element configuration, for the depressurization loss-of-coolant accident (LOCA), for the tritium production elements, and for the divertor of the fusion neutron source, along with a discussion of the secondary system and electrical power performance, are presented in Sec. VII.

II. DESIGN OVERVIEW

II.A. Configuration and Dimensions

The GCFTR-2 is a subcritical, fast, helium-cooled reactor using coated TRU fuel particles embedded in SiC matrix pins. A three-dimensional (3-D) depiction of the reactor and its tokamak fusion neutron source is shown in Fig. 1. The annular reactor surrounds the fusion neutron source on the outboard side.

The detailed dimensions are shown in Fig. 2. The inner radius of the reactor core is 485 cm, the core width is 112 cm (100-cm fuel region), and the core height is 300 cm. The tokamak fusion neutron annular plasma source is on the inboard side of the reactor with a width of 216 cm and a height of 367 cm. As indicated in Fig. 1 but not shown in Fig. 2, a divertor is located on the bottom inboard side of the plasma chamber. The plasma chamber and divertor are scaled down from the International Tokamak Experimental Reactor[6] (ITER) design. A 3.5-cm-thick first wall of the plasma chamber separates the core and plasma regions. Both the plasma and the reactor cores are surrounded by a blanket shield that is 77 cm thick on the inboard side and 79.5 cm thick on the outboard side, which in turn is surrounded by a 6-cm-thick ferritic steel vacuum vessel. This entire annular configuration—reactor, plasma, blanket, shield, and vacuum vessel—is contained within a ring of 16 D-shaped superconducting toroidal field coils, each of 43-cm radial thickness. The vacuum vessel abuts the toroidal field coils on the inboard side. Just inside the torodial field magnets is the central solenoidal magnet of 70-cm thickness. The remaining "flux core" space inside the central solenoid has a radius of 66 cm.

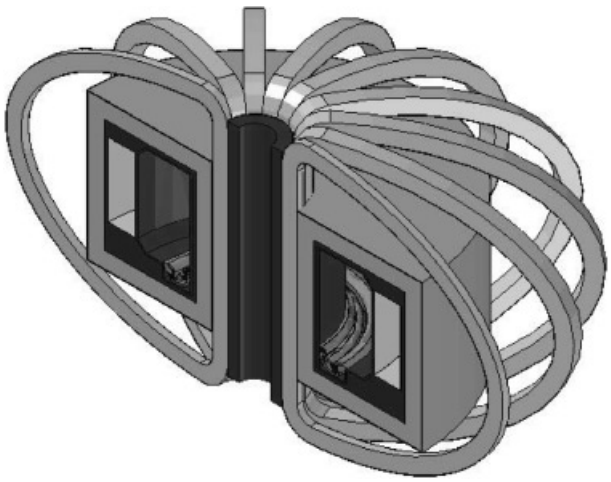

Fig. 1. Three-dimensional depiction of the GCFTR-2.

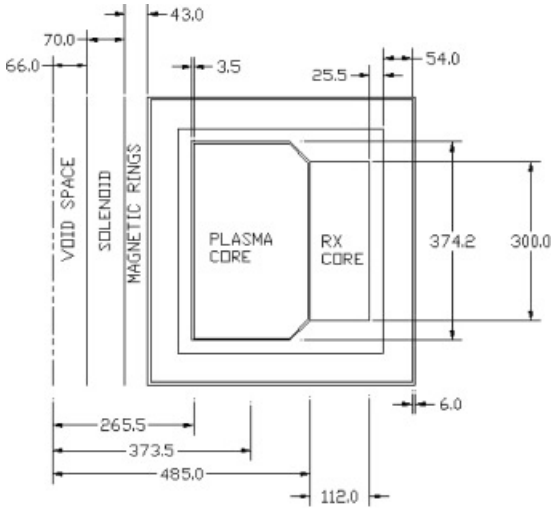

Fig. 2. GCFTR-2 radial dimensions (in centimeters).

II.B Major Parameters and Materials

Table I gives the major parameters and materials used in the GCFTR-2. The fuel parameters and materials were designed for a tri-material isotropic (TRISO) fuel particle that has a TRU kernel surrounded by SiC, C, and ZrC layers, which are embedded in a SiC matrix.

II.C. Performance

The transmutation and electrical performance of the GCFTR-2 are summarized in Table II.

II.D. Radiation Damage and Component Lifetime

Component lifetime against radiation damage is an important consideration. In the reactor core, the lifetime of the TRISO fuel particles is critical to achievement of the deep-burn objective of ≥90% FIMA, which corresponds to a fast (>0.1 MeV) neutron fluence of 6.5×10^{23} n/cm^2 in the GCFTR-2. Unfortunately, there are few data for TRISO particles at deep burnup. The Peachbottom Reactor irradiated TRISO particles with a fast fluence of 1.3×10^{21} n/cm^2 at temperatures of 800 to 1350°C, with a failure rate of 1.4×10^{-6} (Ref. 7). More

TABLE I

Major Parameters and Materials of the GCFTR-2

Parameters and Materials	Values
Reactor core	
Annular dimensions	R_{in} = 4.85 m, R_{out} = 5.97 m, H = 3 m
Fuel/He/structure (vol%)	60/30/10
Fuel element	TRISO particles in SiC matrix, pins d = 1.34 cm
TRU coated particle diameter	660 μm
TRU-oxide fuel enrichment	62%
TRU fuel mass	74 tonnes
Maximum k_{eff}	0.95
He mass flow, He temperature	M = 2870 kg/s, $T_{\text{He}}^{in}/T_{\text{He}}^{out}$ = 280/494°C
Power density, maximum T_{fuel}	q''' = 42.2 MW/m^3, T_{fuel}^{max} = 582°C
Clad/structural materials	Zircaloy-4/HT-9
Fission power	3000 MW(thermal)
Blanket shield	
Shield materials	HT-9, He, B_4C, HfC, Ir, WC, Cd, Pb, Xe
Tritium breeder	Li_2O
Inboard/outboard thickness	77/79.5 cm
Tritium breeding ratio	1.1
Plasma	
Plasma current	8.3 MA
Fusion power/neutron source rate	50 MW/1.8 $\times$ 10^{19} s^{-1} to 180 MW/6.5 $\times$ 10^{19} s^{-1}
Fusion gain ($Q_p = P_{fus}/P_{plasma\ heating}$)	180 MW(thermal)/58 MW(thermal) = 3.2
Superconducting magnets	
Field central solenoid, toroidal field coils, toroidal field on center of plasma	12.4 T, 11.8 T, 5.7 T
Divertor	
Materials	W tiles on CuCrZr, He cooled
Heat flux	$\leq$2.0 MW/m^2
First wall	
Materials	Be on HT-9, He cooled
Neutron wall load (14 MeV)	$\leq$0.6 MW/m^2
Heat flux	$\leq$0.23 MW/m^2

recent results from development programs in the United States and Germany have achieved burnups as large as 80% FIMA and fast neutron fluences as large as 1.2 $\times$ 10^{22} n/cm^2, with failure rates of 10^{-4} to 10^{-6} for the higher FIMA U.S. tests and 10^{-7} to 10^{-9} for the order 10% FIMA German tests.[8] A further potential problem is degradation of SiC thermal conductivity with irradiation. Achievement of the fluence lifetimes required for a deep-burn transmutation reactor such as GCFTR-2 is a major challenge for fuel development.

The fuel cladding and fuel assembly structure lifetimes against radiation damage are also important considerations. The minimal requirement for the Zircaloy clad is an acceptable level of swelling during the

TABLE II

Transmutation and Electrical Performance of GCFTR-2

Parameter	Value
TRU burnup objective	$\geq$90% FIMA
TRU transmutation rate	1100 kg/full-power year (FPY)
SNF transmutation rate	99.3 tonnes/FPY
LWR support ratio	Three 1-GW LWRs per GCFTR
Fission thermal power	3000 MW(thermal)
Gross electrical power	1020 MW(electric)
Net electrical power	700 MW(electric)
Electrical power amplification, Q_e	3.2

five-batch residence time of 8.1 yr, which corresponds to a fast neutron fluence of 5.1×10^{22} n/cm^2. We have been unable to find data on Zircaloy radiation damage lifetimes, but such must exist. The lifetime of the ferritic steel structure can be estimated from the values of 80 to 150 displacements per atom (dpa) quoted for HT-9 (Ref. 9), which corresponds to 1.5 to 3.0×10^{23} n/cm^2 fast neutron fluence. For 40 yr of operation at 75% availability, the accumulated fast neutron fluence in the core would be 4.0×10^{23} n/cm^2, indicating that one or two replacements of the fuel assembly structure would be necessary.

The plasma chamber "first wall," which consists of 3 cm of ferritic steel, would receive a fast neutron fluence of 7.5×10^{23} n/cm^2 over 30 effective full-power years (EFPYs) of operation. Using the same estimate for the radiation damage lifetime of ferritic steel as above, this would require two to four first wall replacements.

The shield was designed to protect the superconducting magnets from radiation damage failure over the 30-EFPY lifetime.

The ITER divertor,[6] after which the GCFTR-2 divertor is modeled, is expected to require replacement eight times during the ITER's lifetime because of plasma erosion of the surface. The plasma flux to the divertor in the ITER is a few times greater than that in the GCFTR-2, but the GCFTR-2 lifetime is several times longer than that of the ITER, so tens of divertor replacements might be anticipated for the GCFTR-2.

The radiation damage and lifetime estimates are summarized in Table III.

III. FUEL SYSTEM

III.A. SNF Reprocessing

It is necessary to know the composition of the transuranic fuel that will be available from SNF in order to design the GCFTR-2; thus, it is necessary to specify the initial SNF composition and the SNF reprocessing system. The solvent extraction system used is the four-part partitioning process using the DIDPA and TBP solvents as designed by Kubota et al.[11] at JAERI. A process that would utilize UREX, TRUEX, and DIAMEX was also considered; however, for the simplicity of system design and superior separation factors, the DIDPA process was chosen despite a tendency for quicker solvent degradation compared with the other possible solvents.[12–15]

The four-part process will separate the Np and Pu, U, Am and Cm, and lanthanides into four separate solutions that can be recombined into any desired combination as dictated by the thermal and reactor physics aspects of the core. There will be a small amount of residual uranium in the system due to the imperfection of the process but not nearly enough to affect the kernel. The separation efficiencies for the DIDPA process are shown in Table IV.

Since the efficiencies are so high, the amount of lanthanide poisons present in the minor actinide stream is low enough that there will be little to no effect on the fuel utilization factor. With the desired elements separated, the uranium stream can divert back into LWR fuel processing since much of it is still enriched and useful, and

TABLE III

Component Radiation Damage Lifetimes

Component	GCFTR-2 Fast Neutron Fluence (n/cm^2 > 0.1 MeV)	LIMIT Fast Neutron Fluence (n/cm^2 > 0.1 MeV)	Replacement over 30-EFPY Core Life
Reactor core			
Clad over five-batch burn	5.1×10^{22}	?	After each five-batch residence?
Structure over 30 EFPYs	4.0×10^{23}	1.5 to 3.0×10^{23} [a]	One to two replacements
TRISO fuel particle			
At 23% FIMA (five batches)	1.1×10^{23}	?	
At 90% FIMA	6.5×10^{23}	?	Lifetime component goal
Fusion neutron source			
TFC Nb_3Sn 30, EFPYs	3.6×10^{18}	1×10^{19} [b]	Lifetime component goal
TFC insulation, 30 EFPYs	4.7×10^{7} rad	10^9 to 10^{10} rad[b]	Lifetime component goal
First-wall, 30 EFPYs	7.5×10^{23}	1.5 to 3.0×10^{23} [a]	Two to four replacements
Divertor		Plasma erosion	Tens of replacements

[a]Reference 9.
[b]Reference 10.

TABLE IV

Separation Properties of Four-Part Partitioning Process*

Elements	Target Recovery (%)	Separation Efficiency (%)	Estimated Recovery (%)
Np	99.5	>99.95	99.85
Pu	99.9	>99.99	99.85
Cm	99.99	>99.99	99.97
Am	99.9	>99.99	99.97

*Reference 11.

the lanthanides and fission products will be sent to a waste vitrification process and then to a repository.[16] The remaining isotopes of Np, Pu, Am, and Cm will be separated from the aqueous streams and then combined, oxidized, and sent to the TRISO kernel manufacturing stage of the fuel cycle. The final number densities are shown in Table V.

TABLE V

Number Densities of TRU*

Isotope	Number Density (10^{24} atoms/cm^3)
^{237}Np	1.06E−03[a]
^{238}Pu	3.03E−04
^{239}Pu	1.31E−02
^{240}Pu	5.15E−03
^{241}Pu	9.35E−04
^{242}Pu	1.12E−03
^{244}Pu	3.80E−08
^{241}Am	2.21E−03
^{242m}Am	1.60E−06
^{243}Am	2.45E−04
^{242}Cm	4.20E−09
^{243}Cm	4.24E−07
^{244}Cm	2.75E−05
^{245}Cm	2.97E−06
^{246}Cm	2.35E−07
^{247}Cm	2.37E−09

*Reference 17.
[a]Read as 1.06×10^{-3}.

III.B. Coated Fuel Particles

The two types of fuel particles that were considered for the design were the TRISO and the bi-material isotropic (BISO). The TRISO fuel particle is composed of a TRU kernel, a buffer layer, and three structural layers that provide containment for the fuel and its fission products. The BISO differs from the TRISO particle by having one less structural layer. Because of having one less layer, the BISO particle is smaller than the TRISO particle. From a fuel point of view, the BISO particle would be a good choice for use in the GCFTR-2 if a zirconium-based matrix material was used; however, the TRISO particle was chosen over the BISO since the TRISO/SiC matrix had more advantageous reactor physics properties and a more resilient structure for longer-term burnup. A representative TRISO particle is shown in Fig. 3.

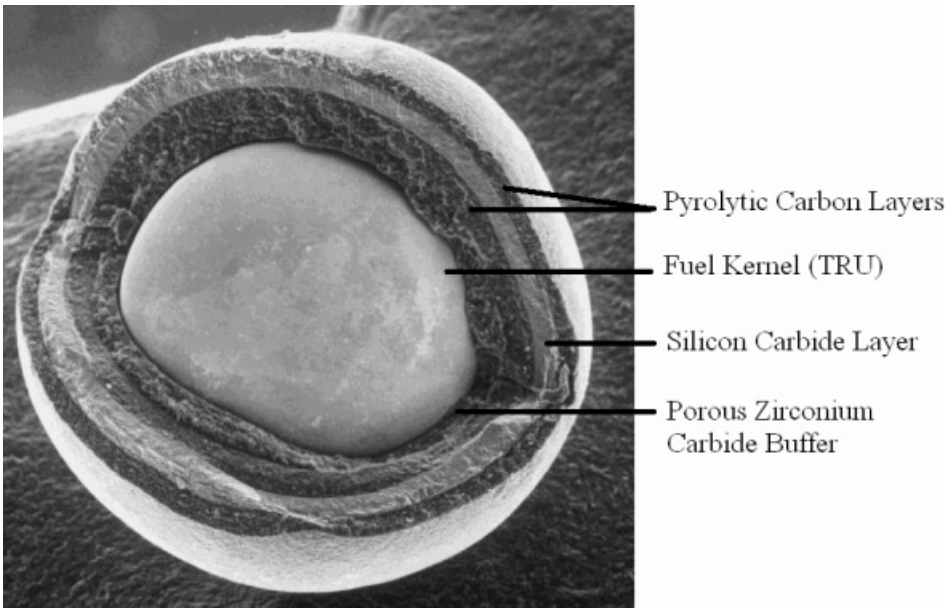

Fig. 3. Representative TRISO particle.[18]

The first of the three structural layers of the TRISO particle is the inner pyrolytic carbon (IPyC) layer. This layer is essential, because during the coating processes of the TRISO, chlorine is used, and this layer protects the kernel from exposure to chlorine. The next layer is composed of SiC. When the TRISO undergoes irradiation, the kernel and buffer layers will expand outward, and this layer will contract, which balances the inner and outer pressures. The last layer is the outer pyrolytic carbon (OPyC) layer. This layer protects the SiC from interacting with the outside materials (cladding, matrix, etc.).

The TRISO particle is used in the design of the GCFTR-2 since it will allow for high degrees of burnup as well as aid in the disposal process of spent fuel.

The next area of concern is the form of the TRU fuel kernel. Options include oxide, carbide, and oxy-carbide kernels. Each choice was compared, and the pros and cons were weighed. The oxide kernel is advantageous since it has low volatility losses of americium, and producing oxide kernels is a well-known process. The two largest problems with oxide kernels are kernel migration (amoeba effect) and pressure buildup from carbon monoxide gas. The carbide kernel does not have any unfavorable pressure buildup or thermal migration issues. However, it has other severe problems, namely, volatility with americium during fabrication and an unfavorable reaction with SiC (the first layer of the particle). The benefits of the oxy-carbide kernel are similar to the benefits of each, the oxide and the carbide kernels; however, americium volatility is still unacceptably high.[19] The volatility with americium is unacceptable since americium is a major constituent of the TRU composition. This leaves two choices: oxide or nitride kernels. The production of ^{14}C by neutron capture is a disadvantage of the nitride kernels, which led us to rule them out. Thus, the oxide kernel used in the previous GCFTR design[5] was chosen, with the recognition that its problems must be resolved. The actinide composition of the TRISO kernel is listed in Table VI.

To minimize the pressure buildup of carbon monoxide in the TRISO particle, a buffer layer of ZrC was proposed,[20] since Zr is an "oxygen getter," with oxygen having a greater affinity toward it than toward carbon. The zirconium not only alleviates carbon monoxide buildup, but it also can help to minimize thermal migration since carbon monoxide creates hot spots, which lead to thermal migration of the kernel.[20] Furthermore, the ZrC layer acts as a buffer for the recoil of fission products, and it is porous, which aids in containing the fission gases. The physical properties of the materials in a TRISO particle are given in Table VII. A diagram of the TRISO particle used in the GCFTR-2 design is shown in Fig. 4.

TABLE VI

TRISO Kernel Composition*

Element	Weight Percent	Oxide Form	Melting Point (°C)
Uranium	0.43	UO_2	2820
Neptunium	4.32	Np_2O_3	2510
Plutonium	84.91	Pu_2O_3	2085
Americium	10.21	Am_2O_3	2190
Curium	0.13	Cm_2O_3	2225

*Reference 5.

TABLE VII

Physical Properties of TRISO Fuel Particle Components*

Material	Melting Point (°C)	Thermal Conductivity (W/m·°C)	Density (g/cm^3)
TRU kernel	2085	2.75	10.63
PyC	2546	3.50	1.85
ZrC buffer	3250	20.00	1.10
SiC	3373	960.00	3.2

*Reference 21.

III.C. Fuel Configuration

Two possible fuel element configurations were investigated: (a) a fuel pin consisting of the fuel particles embedded in a SiC matrix and clad with Zircaloy-4 (Ref. 5), seen in Fig. 5, and (b) solid blocks of low-density graphite foam[22] (LDGF) with the fuel pellets embedded, as suggested in Ref. 23 and shown in Fig. 6. The fuel pin diameter was 1.34 cm with a hexagonal pitch of 1.417 cm. The hexagonal fuel assembly was 36.625 cm wide and 300 cm tall. The dimension across flats of the hexagonal LDGF fuel block was taken as the same as the pin fuel assembly for comparison purposes.

A hexagonal fuel assembly is envisioned for the fuel pin configuration, with Zircaloy-4–clad fuel pins containing the TRISO pellets embedded in a SiC matrix material using the isothermal forced flow chemical vapor infiltration (CVI) method.[24] This CVI method, which is only feasible for short distances because of potential blocking of the tubes when the SiC propagates through the packed TRISO particles, requires that a short, cylindrical pellet be created, so the fuel pin will be made up of a stack of pellets ~5 cm (~2 in.) in length. The maximum packing factor for this geometry is 62%; however, a realistic value may be more like 50 to 60%. The SiC matrix adds extra protection, in addition to the TRISO particle, against gaseous fission product release. Following the creation of the pellets, the Zircaloy-4 cladding will then be filled with pellets and hermetically sealed as yet another barrier to gaseous fission product release.

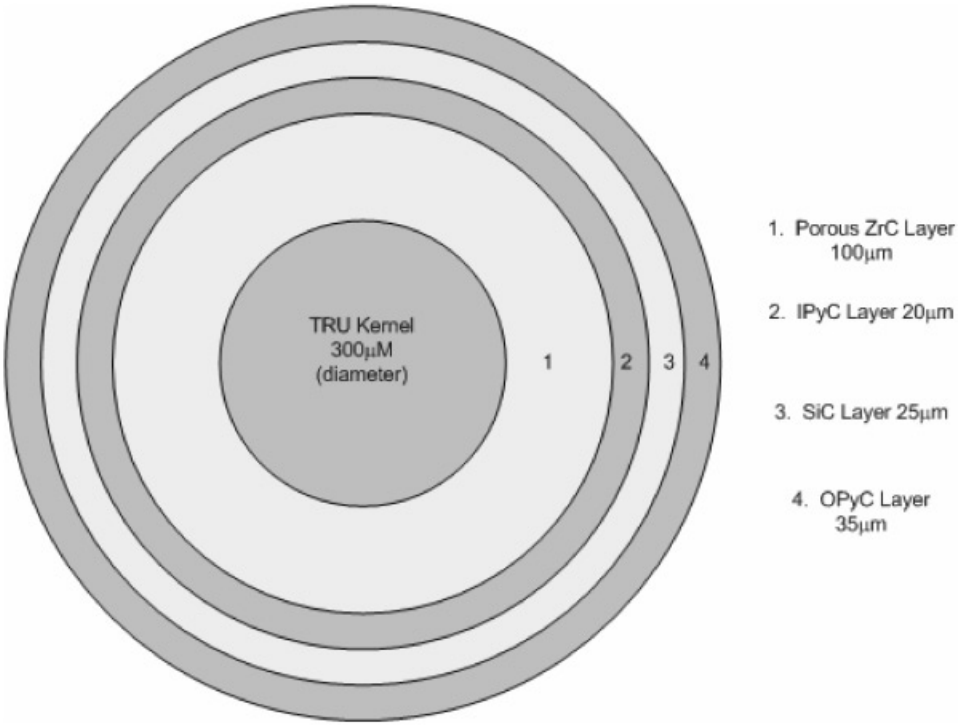

Fig. 4. TRISO particle for GFCTR-2 (Ref. 5).

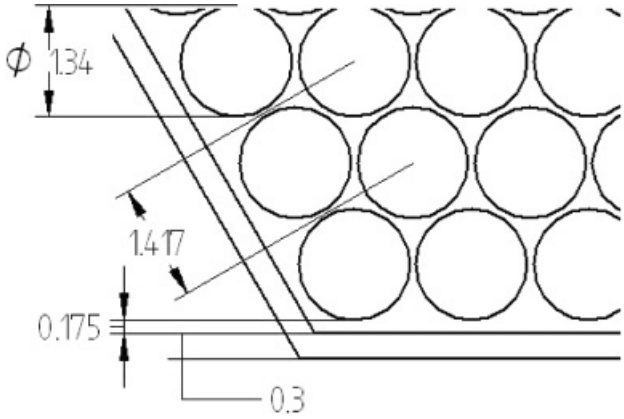

Fig. 5. Fuel pin assembly cutaway (in centimeters).

The other design considered was an LDGF block with embedded TRISO particles. The block resembles a fuel assembly of a high-temperature gas-cooled reactor with a central coolant channel. The physical properties of LDGF and SiC are compared in Table VIII. The low number density of the LDGF was initially viewed as an advantage in that it would not soften the fission neutron spectrum as much as the higher density of SiC; however, this turned out not to be an unmitigated advantage because of the larger material damage effect of faster neutrons.

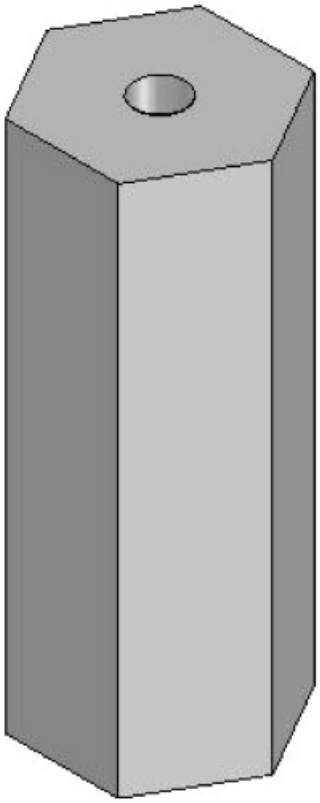

Fig. 6. LDGF block assembly with central cooling channel.

TABLE VIII

Physical Properties of Fuel Materials*

Property	LDGF	SiC
Density (g/cm^3)	0.25 to 0.65	3.1
Thermal conductivity (W/m·K)	~0.3 to 175	120
Thermal diffusivity (cm^2/s)	0.01 to 4.53	1.6
Coefficient of thermal expansion (/K)	~0	4
Tensile strength (MPa)	0.7 to 1.6	2700
Compressive strength (MPa)	1 to 3.5	3900
Compressive modulus (GPa)	0.144	1.05

*References 25 and 26.

The thermal performance of the SiC fuel pins and LDGF fuel blocks were calculated, as described in Sec. VII. Under nominal operating conditions there is little difference between the two fuel options. The maximum temperature reached by the LDGF fuel block in a LOCA is ~2975 K, comparable to the value for the SiC fuel pins. This temperature exceeds the melting point of TRU-oxides (2308 K) and of the Zircaloy clad on the fuel pins (2118 K). At these temperatures, the fission gas pressure buildup within the TRISO particles themselves may cause the particles to fail, as will be discussed in Sec. III.E. Therefore, there is little difference in the thermal performance of the SiC fuel pins and the LDGF fuel blocks.

However, there are two other major issues with the LDGF: (a) The relatively brittle nature of the material raises the question of the inability of the lower portion of the fuel assembly to support the weight of the upper portion,[25] which could necessitate extra structural material for support, and (b) the LDGF fabrication process is based on the graphitization process, in which the foam is heated twice to extremely high temperatures nearing 3000 K (Ref. 22), which exceeds the melting point of the TRU kernel in the TRISO particle. There is also a lack of long-term durability data for the LDGF. For these reasons, the TRISO/SiC fuel pin clad with Zircaloy-4 was chosen as the reference fuel configuration.

III.D. Fuel Manufacturing

The sol-gel process[8,15,27,28] would be used to manufacture the actinide fuel kernels. The process begins by preparing the sol, which includes the TRUs to be transmuted, and placing it into the device designed to form uniform droplets of fuel. The droplets are formed by forcing the solution into a hypodermic needle through an interchangeable nozzle (see Fig. 7). Once the droplets are formed, the droplets would be formed into a wet "gel." Gelation is a fast reaction since it takes place by the action of ammonia on sols, which are stabilized by hydrogen ion adsorption.[15] During the gelation phase, the droplets form a stabilizing barrier that surrounds the droplet. Once gelation is complete, the droplets are washed with water to remove the ammonium nitrate. Once the washing is completed, the fuel kernels would then be dried using superheated steam. This process takes ~10 min and occurs at 250°C. Superheated steam is used since it has been found that the relatively dense, water-washed gel kernels can be dried without cracking if the drying takes place in a wet atmosphere.[15] After the drying phase, the sintering begins. The droplets are sintered with a prescribed temperature program and reduced until the kernels are ready for layering. The fuel kernels are heated to 1300°C for a duration of 3 h. The droplet formation process is displayed in Fig. 7.

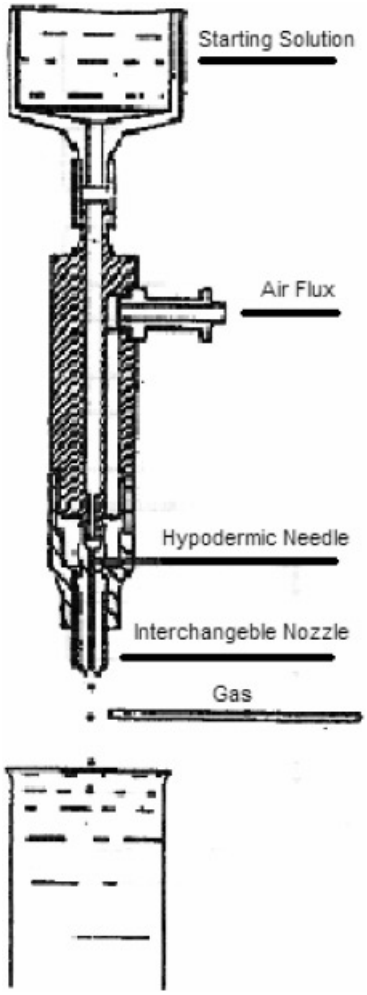

Fig. 7. Droplet formation.[15]

Following the sol-gel process for forming the fuel kernel, the fuel particle will be constructed. To form the TRISO particle needed for the GCFTR-2, a process known as CVI or chemical vapor deposition is used. CVI adds the coatings to the fuel kernel. These layers include the porous zirconium carbide buffer, the inner dense

pyrolytic carbon, the silicon carbide, and the outer dense pyrolytic carbon layer. CVI uses a gas stream that reacts on the surfaces of a porous body to deposit matrix material. By using this method, high-temperature phases can be produced at temperatures below their melting points.[27] The ZrC coating will be formed based on the in-situ generation of zirconium halide vapor, hydrocarbon, and hydrogen. Among the processes that have been developed, the bromide process is the most convenient. This involves the bromine, which is liquid at room temperature, to be reacted to generate $ZrBr_4$ vapor, which was then mixed with the other coating gases, CH_4 and H_2. This deposited the ZrC layer onto the particle. The fabrication process by CVI of a stoichiometric ZrC coating layer has been established based on the in-situ generation of zirconium halide vapor.[28] Following the ZrC buffer layer was the IPyC layer, which was formed by depositing a mixture of acetylene, propylene, and argon at 1230°C. Following the IPyC coating is the SiC coating. The SiC layer is deposited using CVI using a mixture of hydrogen and methyltrichlorosilane at 1650°C (Ref. 8). The remaining layer to be coated onto the particle is the OPyC layer, which uses CVI as well. This fuel fabrication flow is shown in Fig. 8.

III.E. TRISO Particle Lifetime

The fission gases present in the fuel play an important role in the process of degradation of fuel raised to high temperature. During this operation, global swelling of fuel is produced by the enclosed gases and the internal overpressure due to intergranular gas bubbles. This leads to splitting of fuel along grain boundaries.[29,30]

The ORIGEN code[31] was run for deep burn up to 90% burnup at a nominal centerline temperature of 535°C. Assuming 50% porosity in the buffer layer of 100 μm (Refs. 5 and 26), the pressure buildup shown in Fig. 9 was calculated.

The main contribution to this buildup is from He, Kr, I, Xe, and Br. The maximum pressure that the fission gases will reach at the nominal operating temperature is ~150 MPa, which is much less than the compressive yield strength of 345 MPa for SiC (Ref. 5). Figure 9 also provides a measure of the tolerable decrease in SiC yield strength due to radiation damage at the nominal operating condition, or a measure of the tolerable reduction in composite fuel thermal conductivity due to radiation damage, both a factor of ~2.5. We note that the thermal conductivity of SiC has been observed to significantly degrade under fast neutron irradiation. Hence, it can be inferred that the fuel particle will retain its integrity (radiation damage effects aside) at the nominal operating temperature during the 90% burnup period. The ratio of 345 MPa to the nominal pressure shown in Fig. 9 times 535°C provides an estimate of the maximum fuel temperature that could be withstood under accident conditions without failure of the TRISO fuel particles.

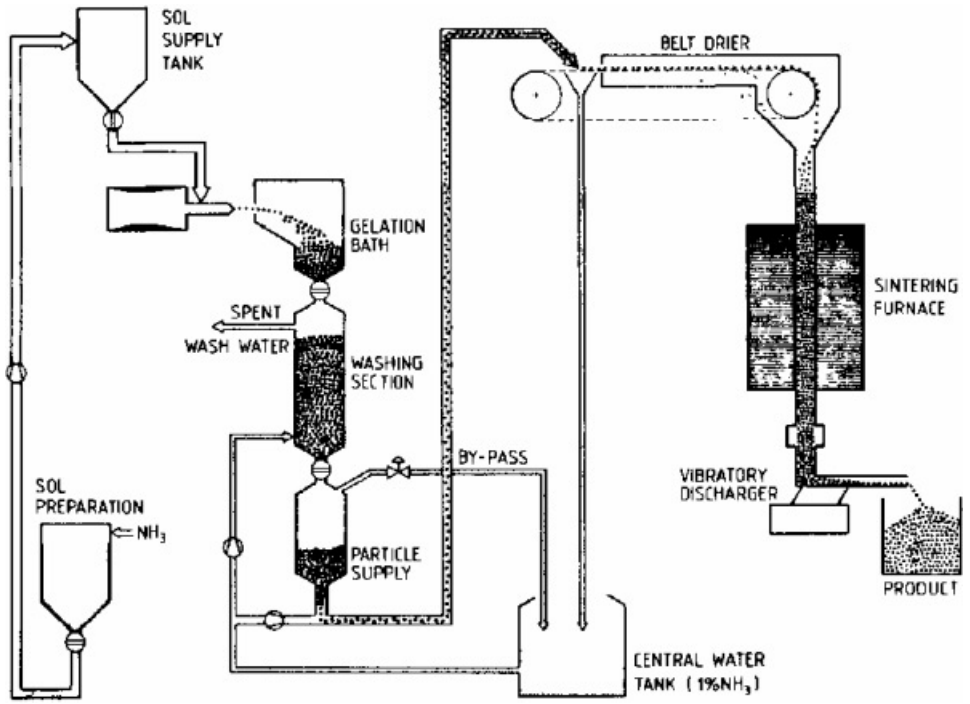

Fig. 8. Fuel fabrication flow.[15]

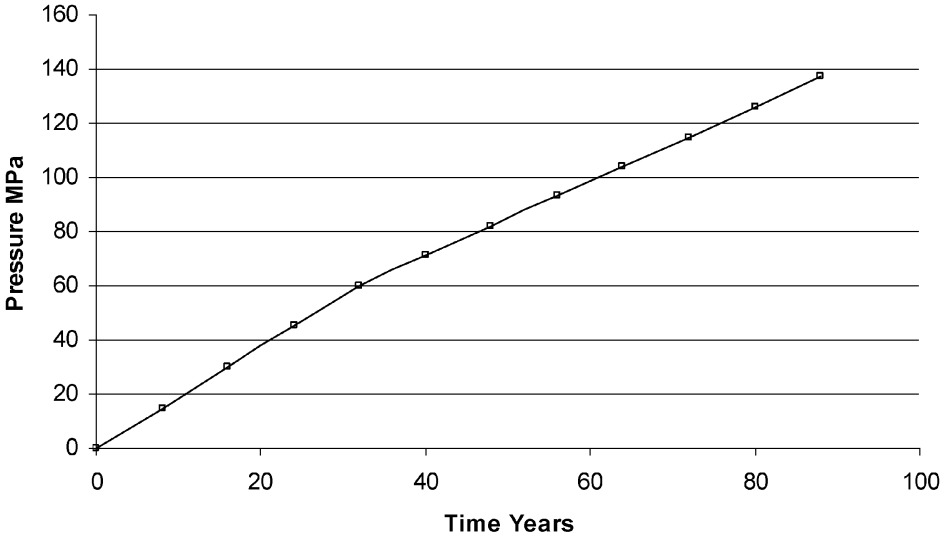

Fig. 9. Gas pressure buildup in TRISO particle at nominal operating temperature of 535°C.

III.F. Waste Storage

Most of the waste that will be produced after the deep burnup can be handled with the shielding provided by the waste package. It will be contact handled, which means that the waste would not require remote handling, since alpha particles and beta particles would not penetrate the walls of the package. However, some of the containers with traces of gamma generators (e.g., Cs) will have to be remotely handled.[32,33]

The waste could be vitrified by a slurry-fed ceramic melter system. The waste would be mixed with molten glass and discharged from canisters where it solidifies. The reasons glass is chosen are that it has high solubility for the nuclides found in high-level waste, shows resistance to radiation damage, and requires only moderate temperature borosilicate glass based on the properties given in Table IX.

TABLE IX

Physical Properties of Borosilicate Glass*

Property	Value
Thermal conductivity at 100°C	0.55 Btu/h·ft·F
Heat capacity (100°C)	0.22 cal/g·°C
Fractional thermal expansion	1.22×10^{-5}/°C
Young's modulus	9.0×10^{9} psi
Tensile strength	9.0×10^{3} psi
Compressive strength	1.0×10^{5} psi
Poisson ratio	0.2
Density (100°C)	2.5 to 3.0 g/cm^3

*Reference 34.

Several materials are available for the canister in which vitrified waste is to be placed. They are Type 304L stainless steel, plated carbon steel, titanium, and recycled contaminated steel. Overall, Type 304L is the most promising material based on the experiments performed on the materials mentioned above. Type 304L is an extra-low-carbon and high-chromium-content alloy. The 0.03% maximum carbon content eliminates carbide precipitation due to welding. Consequently, the alloy can be used in the "as welded" condition even in severe corrosive conditions.[35]

The typical size of a canister will be 3.0 m high with a 0.60-m outer diameter and a wall thickness of 9.53 mm. Each canister can hold ~1700 kg of glass, of which ~45 kg will be radionuclides. The canister can withstand decay heat of ~700 W (well above the decay heat calculated with the ORIGEN code, ~20 W in 30 yr), and the maximum activity of ~300 kCi would produce a radiation level of ~550 rem/h on contact. The canister would normally be expected to corrode in 300 yr, but in this case that is unlikely since there will not be enough heat to generate steam to cause corrosion.[34]

IV. NUCLEAR DESIGN

IV.A. Fuel Configuration

The goal of the GCFTR-2 is to achieve deep burn (>90%) of the actinide fuel with little or no reprocessing. To realize this goal a fast neutron spectrum is desired in order to make use of the high fission-to-capture ratio present with most actinides. There is, however, an inherent trade-off since a harder neutron spectrum increases the probability of radiation damage to the nonfuel structure

of the core. It is necessary to choose a fuel assembly design that maximizes the rate of actinide fission with respect to the rate of radiation damage.

As described in Sec. III, the TRISO and BISO coated fuel particles are being considered for the GCFTR-2 fuel. These particles would be embedded in a matrix material such as SiC or Zircaloy, respectively. A recently developed LDGF (Ref. 22) was also considered as the matrix material. In addition to having excellent thermal conductivity properties, the graphite foam has a very low density, which will produce a harder neutron spectrum.

The four fuel configurations under consideration are (a) fuel pins of TRISO particles embedded in a SiC matrix, (b) fuel pins of BISO particles embedded in a Zircaloy matrix, (c) TRISO particles embedded in graphite foam blocks, and (d) BISO particles embedded in graphite foam blocks. Configurations 1 and 2 consist of Zircaloy-clad fuel pins with helium coolant flowing around them, as depicted in Fig. 5. Configurations 3 and 4 are fuel block designs that have helium coolant channels running vertically throughout the blocks, as depicted in Fig. 6. The fuel will occupy ~60% of the core volume, leaving ~30% coolant volume and ~10% structural volume.

The eigenvalue and core-averaged flux for each of these fuel configurations was computed using the radiation transport code EVENT (Ref. 36). The entire reactor was modeled using two-dimensional (2-D) *r-z* geometry with 34-group cross sections generated by MC-2 (Ref. 37). A P_5 angular approximation was used to calculate the neutron flux. Each region of the reactor was homogenized by a simple uniform smearing of the volume-weighted material composition. It was assumed that the fusion neutron source is isotropic and uniform inside the plasma chamber. Therefore, the fusion source was modeled by placing the isotropic volumetric source in the first wall. Representative neutron spectra in the core are shown in Fig. 10.

From a neutronic standpoint, the basis of comparison between the assembly types is the neutron utilization index[5] (NUI), defined as the total fission rate divided by the neutron flux with energy >100 keV. The assembly with the highest NUI should provide the most fissions per fast neutron, i.e., the most actinide burn per neutron capable of inducing structural damage. The NUI for each assembly is shown in Table X along with spectral parameters. The configuration with the highest NUI is the assembly with pins of TRISO particles embedded in SiC. For this and other reasons discussed in Sec. III, this fuel configuration was selected for the GCFTR-2 and considered exclusively in the design analysis discussed hereafter.

IV.B. Assembly Design and Fuel Enrichment

The TRISO/SiC pins are roughly the same size as pressurized water reactor (PWR) pins, with an outer pin diameter of 1.34 cm. The pins are clad with Zircaloy-4 and tightly arranged in hexagonal assemblies with a pin pitch of 1.417 cm. The hexagonal assemblies are placed immediately outside the first wall, completely circumscribing the plasma chamber, as shown in Fig. 11. The fuel pin and assembly parameters are given in Table XI.

Since the isotopic composition of the TRU in the fuel particle kernels does not include uranium, the conventional definition of fuel enrichment does not apply to the GCFTR. Here, enrichment refers to the volume of the coated fuel particles divided by the total volume of the fuel, which includes the fuel particles and the matrix

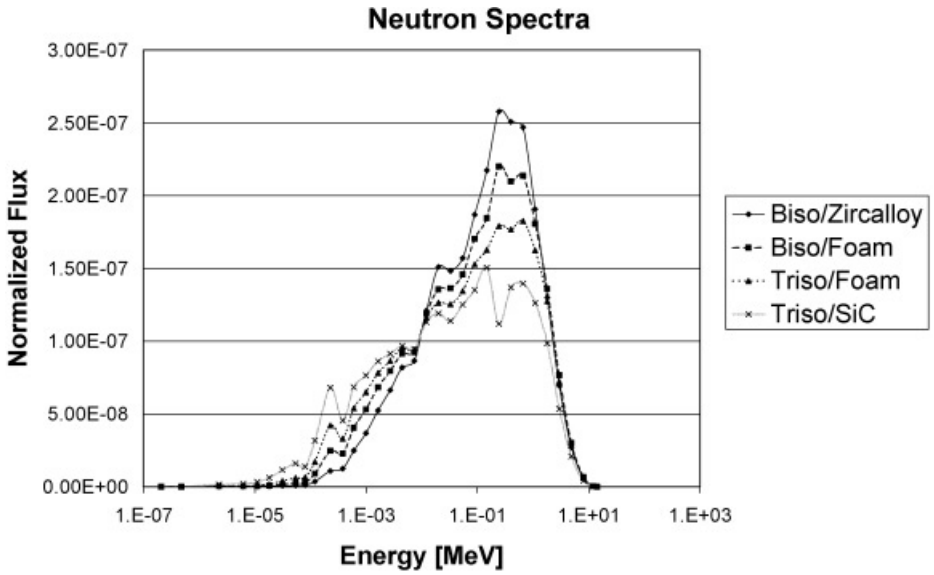

Fig. 10. Neutron spectra with different fuel configurations.

TABLE X

Fuel Configuration Comparison

	TRISO/SiC	BISO/Zircaloy	TRISO/LDGF	BISO/LDGF
k_{eff}	0.950	0.938	0.950	0.950
Fast neutrons[a] (%)	45.22	62.35	53.51	58.18
Intermediate neutrons[b] (%)	54.71	37.65	46.48	41.80
Thermal neutrons[c] (%)	0.07	0.01	0.02	0.01
NUI ($\times 10^{-6}$)	12.83	4.01	7.67	5.43

[a]20 MeV to ~100 keV.
[b]100 keV to ~6 eV.
[c]<6 eV.

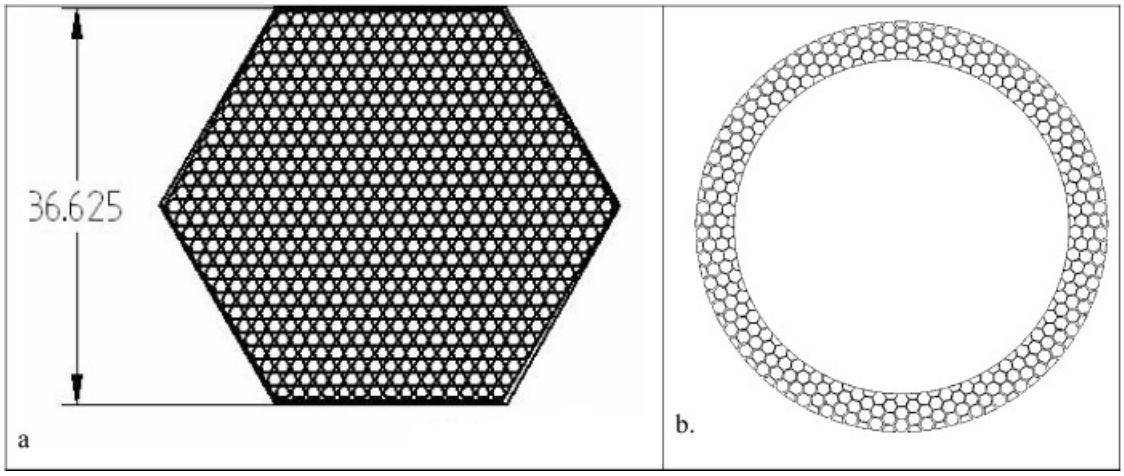

Fig. 11. Fuel assemblies (in centimeters): (a) single fuel assembly and (b) core layout.

TABLE XI

Fuel Pin and Assembly Parameters

Flat-to-flat distance	36.625 cm
Pin diameter with clad	1.34 cm
Clad thickness	0.06 cm
Pin pitch	1.417 cm
Assembly wall thickness	0.3 cm
Pins/assembly	631
Total pin count for core	185 000

material. In other words, the fuel enrichment is equivalent to the packing fraction of the TRISO particles in the matrix material. Because of the low delayed neutron fraction of ^{239}Pu and some of the other actinides, the GCFTR-2 will operate at subcriticality with $k_{eff} \leq 0.95$ to enhance the reactivity margin to prompt critical. For the core shown in Fig. 11 with the TRISO/SiC fuel pin, a fuel/coolant/structure volume percentage of 60/30/10 and a height of 3 m, $k_{eff} \approx 0.95$ requires a core fuel enrichment of 38.5%. As discussed below, a higher fuel enrichment is needed to offset the addition of Li_2O for tritium breeding (and of the Zircaloy cladding, which was omitted in the above calculation).

IV.C. Tritium Production

The subcritical GCFTR-2 is driven by a deuterium-tritium fusion neutron source. It is necessary to achieve a condition of tritium self-sufficiency, where the reactor produces enough tritium to independently sustain the fusion source. Tritium production is accomplished utilizing the (n, α) neutron capture reaction in lithium. The condition for tritium self-sufficiency can be characterized in terms of the tritium breeding ratio (TBR), defined as follows:

$$\text{TBR} = \frac{\text{Number of tritium produced per unit time}}{\text{Number of fusion source neutrons per unit time}} .$$

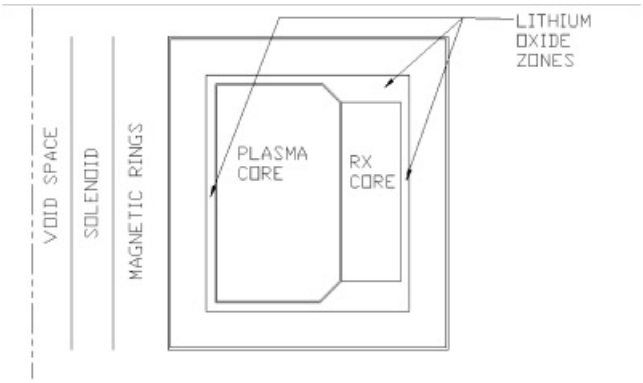

Fig. 12. Location of lithium oxide for tritium production.

As discussed in Sec. VI, taking into account the loss of tritium in the extraction process and the loss due to the radioactive decay, tritium self-sufficiency requires TBR $\approx$ 1.1.

The tritium production reaction is the neutron capture reaction by lithium. A calculation was made in which 90% enriched (in ^{6}Li) Li_2O was placed in the upper and outboard of the reflector, and 30% enriched Li_2O was placed in the inboard of the reflector, as indicated in Fig. 12. Li_2O was selected in order to obtain the highest lithium number density. It was found that it was also necessary to place some Li_2O inside the core in order to obtain TBR $>$ 1.0. Figure 12 shows the reactor configuration for the calculation, and Table XII gives the parameters used in the calculation.

TABLE XII

Core and Surrounding Reflector Material Composition

Material	Reflector Without LiO_2 (%)	Blanket with LiO_2 (%)	Core (%)
HT-9	70.0	10.0	5.0
He coolant	30.0	40.0	30.0
Lithium oxide	0.0	50.0	0.2
TRU/SiC fuel pin	0.0	0.0	64.3

The TBR was calculated using EVENT in a manner identical to the core calculations described in Sec. IV.A. Replacing 0.1 to 0.2 vol% of the fuel in the core with Li_2O, in addition to the Li_2O in the reflector, resulted in TBR = 1.06 to 1.23. To maintain k_{eff} = 0.95 with 0.1 to 0.2 vol% Li_2O and the cladding in the core, the TRISO fuel enrichment must be increased to 60.0 to 62.5%, which is at the theoretical limit.

IV.D. Reactivity Coefficients

Several key reactivity parameters were computed for the GCFTR-2 with the different fuel configurations under consideration. The two reactivity worths of primary

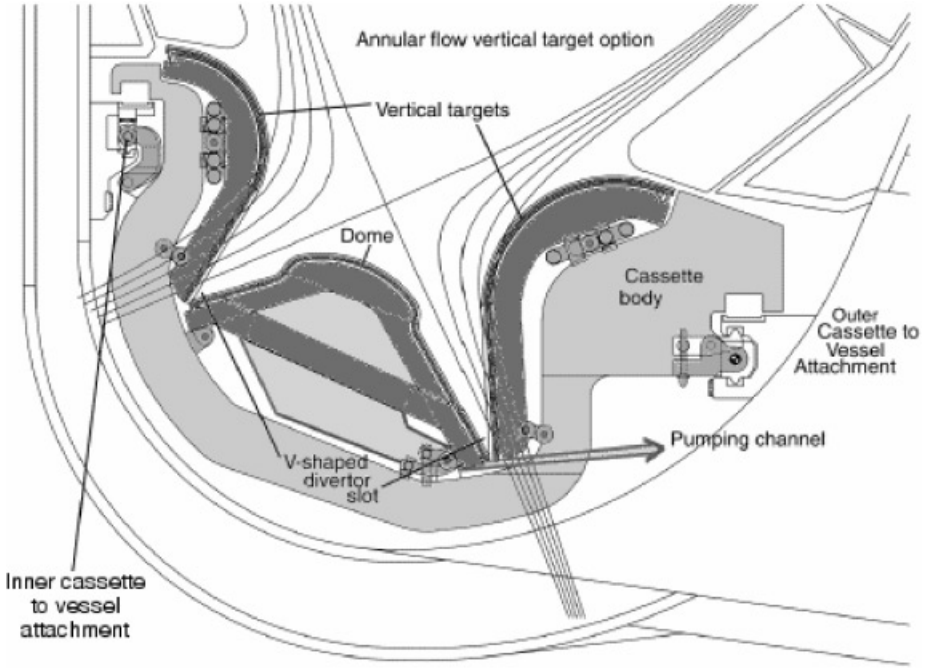

Fig. 13. Detailed drawing of the ITER divertor.[6]

concern are the coolant void reactivity (CVR) and the Doppler temperature reactivity. Each reactivity value was computed by two separate EVENT calculations: one for the nominal reactor under hot operating conditions and the second for a slightly perturbed system.

The CVR was computed by assuming an instantaneous complete voiding of the core coolant, corresponding to the worst-case scenario. The change in reactivity in this scenario is $\delta\rho = 4.963 \times 10^{-4}$, which corresponds to a $\delta k_{eff} = 0.471$ mk (1 mk = 0.001), for the reference TRISO/SiC pin fuel configuration, which has the lowest CVR of the four fuel configurations considered (see Sec. IV.A). Since the helium in the GCFTR-2 acts as a slight neutron moderator, the absence of helium causes a shift in the neutron spectrum toward higher energies, producing a slightly positive CVR.

The Doppler reactivity was calculated by assuming a sudden increase in the fuel and matrix material temperatures. Since there is not a strong presence of resonance absorbers in the fuel, Doppler reactivities were quite low. The reference TRISO/SiC pin fuel configuration had the most negative Doppler reactivity coefficient of $\delta\rho/\delta T_F \approx -5.56 \times 10^{-6}$/°C, or $\delta k_{eff} = -0.00527$ mk per unit increase in fuel temperature.

IV.E. Benchmark

The EVENT calculation used for the above analysis was compared with S_8 TWODANT (Ref. 38) calculations for benchmark purposes. The 34-group cross sections from MC-2 were used in both calculations. The core regions were modeled by volume-weighted material homogenization. Using the diffusion approximation, the EVENT calculation of k_{eff} agreed with TWODANT to within 5.0×10^{-4}.

IV.F. Blanket-Shield Design

In the design of the GCFTR-2, the primary requirements of the blanket shield are to protect the superconducting magnets from radiation damage [maximum allowable fast (>0.1 MeV) neutron fluence 10^{19} n/cm^2, maximum dose to insulators 10^9 rads] so that they can be lifetime components and to produce tritium in lithium-containing tritium breeding elements (TBR ≈ 1.1). Secondary requirements are to reduce the nuclear heating in the superconducting magnets and to reflect neutrons back into the reactor.

There are some additional constraints upon the blanket-shield design. The shielding material should not burn out in the 30 EFPY design lifetime of the GCFTR-2, although the Li_2O will be replaced as necessary. Furthermore, there is an economic incentive to minimize the thickness of the inboard blanket shield and hence the size of the reactor. The inboard shield, vacuum vessel, first wall, and tritium breeding elements were designed to fit into a radial dimension of 82 cm, as indicated in Fig. 2.

The blanket-shield system was modeled in 2-D r-z detailed geometry with MCNP (Ref. 39). The shielding calculation was performed in two stages. The fusion plasma neutron source and the slightly subcritical reactor could not be modeled in a single calculation, so the first calculation treated the high-energy neutron source into the (voided) reactor volume from the 14-MeV plasma neutron source. A fluence tally was used in a voided reactor volume to determine the neutron flux entering the space of the reactor. This fluence number was then scaled by the power at which the fusion source was to be operated. The resulting number gives an input neutron flux for the second stage of the calculation in which the system was modeled as a criticality problem with an initial watt fission spectrum (MCNP manual[40]). The criticality calculation was allowed to converge, and a flux resulting from the average neutron population produced in the core was then taken for all of the areas of importance. The photon source was modeled in a similar manner.

The neutron shielding materials selected for this application deviated somewhat from standard practice in order to achieve a compact configuration. The typical use of B_4C as a shielding material was by and large avoided because, due to the high fast flux and leakage from the reactor, this shielding material would burn out from the n-α reaction if used as the only neutron absorbing material. The alternative selected was a mix of hafnium carbide (HfC) and beryllium as the main shielding materials for neutron absorption with only a small layer of B_4C on the outer edge. Carbon-rich materials were chosen to thermalize the neutrons, which were then absorbed. The shield was designed to operate at 400 to 800°C in the lithium oxide–containing regions to ensure tritium recovery.

NJOY (Ref. 41) was used to broaden the cross sections for all of the runs. NJOY correctly broadens the resonance region and self-shielding cross sections for the materials point to point in energy on a reaction-by-reaction basis. Here, the HfC relies on the resonance n-γ reaction. Solid Li_2O and helium purge gas and a layer of solid beryllium on the outside of the reactor were included for tritium production, as discussed above. At the upper energies of the fission spectrum, where most of the neutron leakage from the core occurs, beryllium has a substantial $n,2n$ reaction. B_4C is used in the outer region of the shield to thermalize and capture the neutrons that propagate to that region. Lastly, a 5-cm-thick sheet of cadmium was added to capture all of the remaining thermalized neutrons.

The photon shielding was a combination of lead, tungsten, and iridium. The tungsten is a good photon shield because of its high atomic number. On the outboard side of the reactor, a 15-cm sheet of lead was added to cut down the photon flux. On the inboard side, space is at an extreme premium, and iridium was chosen to be the photon shield because of it being roughly twice the density of lead.

Tritium breeding was accomplished through a multifaceted approach. The relatively "soft" fast reactor spectrum caused by the large amount of SiC present in the core (Fig. 10) made it infeasible to achieve the required TBR $\approx$ 1.1 with Li_2O located only in the blanket region, even using enrichments of 90% ^6Li. Therefore, Li_2O had to be added to the reactor region. As discussed above, Li_2O was added to the core at 0.2 vol%. MCNP was used to calculate the tritium production and neutron heating in the blanket and core. In addition to highly enriched (90% ^6Li) in the outboard blanket, 30% ^6Li composition lithium was added in the inboard blanket of the fusion chamber in order to utilize the ~14-MeV neutrons that were escaping inward and not contributing to the reactor neutron source. The MCNP calculation yielded TBR $\approx$ 1.1, taking into account the lithium oxide in the core and blanket shield. This MCNP result, together with the more optimistic EVENT calculation of TBR = 1.23 for 0.2 vol% Li_2O in the core and slightly more Li_2O in the blanket, provides confidence that tritium self-sufficiency can be achieved in the GCFTR-2 design.

The blanket-shield design described in Table XIII meets all of the requirements, as indicated in Table XIV. The system fits into the space confines of the superconducting magnets while still keeping the neutron and photon fluxes well below the required levels. With an operating power of 175 MW for the fusion neutron source, the blanket-shield design can last for ~45 yr at 80% availability. This is the point at which the B_4C burns out, after which the neutron flux to the magnets would rapidly increase.

TABLE XIII

Blanket-Shield Dimensions and Materials

Designation	Thickness (cm)	Outer Radius (cm)	Material										
			HT-9 Steel	Be	Ir	Li_2O	HfC	B_4C	WC	Cd	Pb	Xe	He
Outboard													
REFL[a]	3.5	600.5	100%	—	—	—	—	—	—	—	—	—	—
TBE	22	622.5	Four with specifications seen in the subtable below with 90% enriched ^6Li										
SHLD[b]	30	652.5	—	—	—	—	85%	—	10	—	—	5%	—
SHLD	18	670.5	—	—	—	—	—	45%	45%	—	—	10%	—
SHLD	1	671.5	—	—	—	—	—	—	—	95%	—	5%	—
SHLD	5	676.5	—	—	—	—	—	—	—	—	95%	5%	—
VV[c]	6	682.5	100%	—	—	—	—	—	—	—	—	—	—
Inboard													
VV	6	185	100%	—	—	—	—	—	—	—	—	—	—
SHLD	5	190	—	—	95%	—	—	—	—	—	—	5%	—
SHLD	1	191	—	—	—	—	—	—	—	95%	—	5%	—
SHLD	10	201	—	—	—	—	—	45%	45%	—	—	10%	—
SHLD	44.5	245.5	—	—	—	—	85%	—	10	—	—	5%	—
TBE	16.5	262	Three with specifications seen in the subtable below with 30% enriched ^6Li										
FW[d]	3.5	265.5	100%	—	—	—	—	—	—	—	—	—	—
TBE													
	1		—	99%	—	—	—	—	—	—	—	1%	—
	0.5		—	—	100%	—	—	—	—	—	—	—	—
	3.5		—	—	—	95%	—	—	—	—	—	—	5%
	0.5		—	—	100%	—	—	—	—	—	—	—	—

[a]REFL = reflector.
[b]SHLD = shield.
[c]VV = vacuum vessel.
[d]FW = first wall.

TABLE XIV

Shielding Performance*

Parameter	Limit	Calculated Value	Time to End of Life
40-yr fast neutron fluence to superconductor at 75% availability (n/cm^2)	1.0E+19[a]	3.62E+18	≫40
40-yr radiation dose to magnet, insulators at 75% availability (rad)	1E+9/1E+10[b]	4.67E+07	≫40
Nuclear heating per magnet (kW)		5.42E+00	
Total nuclear heating in magnets (kW)		8.64E+01	
Power for cooling toroidal magnets (MW)		9.76E+00	

*Nominal fusion neutron source at 180 MW = 6.39×10^{19} n/s; reactor $k_{eff} = 0.95$.
[a]Read as 1.0×10^{19}.
[b]Epoxy/ceramic.

V. NUCLEAR FUEL CYCLE

V.A. Batch Operation and Fuel Cycle Characteristics

The GCFTR fuel cycle consists of the continuous recycle of TRU fuel until >90% FIMA is achieved. A five-batch shuffling scheme with a 600-day cycle time is used. The core is initially loaded with "fresh" fuel (0% FIMA) and burned for one 600-day cycle. Fuel in the innermost region is then removed from the reactor and allowed to cool, the intermediate regions are each moved to the next inmost region of the core, and the outermost region is filled with fresh fuel. Irradiated fuel will accumulate until after the third cycle, at which time the activity of the first batch to leave the core will have sufficiently decreased. It is then reinserted into the outermost region of the core along with other more reactive pins to compensate for the decreased reactivity due to the previous burn. If necessary, the cladding will be replaced prior to emplacement. It is assumed that the cladding will last for at least one five-batch pass through the reactor. The SiC matrix will be reconstituted as needed and is expected to last for at least one five-batch pass through the reactor.

In the reference scenario, the continuous-recycle case, the TRISO particles are reprocessed after each five-batch exposure in the reactor, their fission products extracted and sent to a high level waste repository (HLWR), and their unburned TRU content refabricated into new particles. In the advanced scenario, the TRISO particles are never reprocessed during this repeated recycling nor before storage in an HLWR at ≥90% FIMA. This advanced scenario depends, of course, on the possibility of developing TRISO particles that can withstand radiation damage to ≥90% FIMA. In either case, the shuffling procedure outlined above will continue until the FIMA for a given batch has reached >90%, at which time the particles will be processed for storage and placed in an HLWR.

The fuel composition in the reactor will change with time until an equilibrium is reached. The equilibrium fuel cycle in the reference scenario consists of fuel in the innermost region that is four times burned, three times burned for the next outermost region, continuing to the outermost region, which is fresh fuel. This equilibrium is an approximation to the true equilibrium, which will consist of a much more diverse assortment of fuel pin burn times.

V.B. Computational Models

Fuel cycle calculations were performed with REBUS-3 (Ref. 42), a fuel cycle depletion code. 34-group cross sections were generated using the MCC-2 (Ref. 37) processing code, the ENDF-B/V cross-section library, and the equilibrium operating temperatures listed in Table XV. Transport calculations were performed with TWODANT (Ref. 38), a 2-D finite-difference flux distribution code, using an S6 approximation. Long-term decay characteristics of processed LWR SNF were

TABLE XV

Transmutation Fuel Cycle Analysis for 3000-MW(thermal) GCFTR-2

Temperature[a] (K)	Region
750	Core fuel
660	Core coolant
700	Core structure
600	Shield
600	Reflector
600	Magnet
600	Central solenoid
600	First wall
600	Vacuum vessel

[a]The coolant temperature for a given region, where not specified, is 50 K less than the temperature of the given region.

calculated using ORIGEN-S (Ref. 31), a depletion and decay code, and KENO V.a (Ref. 43), a criticality code, both of which are included in the SCALE5 package.

V.C. Transmutation Performance with Reference Scenario

The detailed performance metrics for the GCFTR-2 reference scenario are listed in Table XVI. The fusion power swing over a given equilibrium cycle was well within the design limit of 180 MW. The required fuel volume fraction exceeds that possible with equally sized TRISO particles when the packing fraction is taken into account (theoretical maximum ~64%). The 70% figure would be made more realistic if different sized particles were used.

At a thermal power of 3000 MW/FPY, the GCFTR-2 transmutes ~1.11 tonnes of TRUs, which is equivalent to the TRU production rate of three 1000 MW(electric) LWRs per FPY. Hence, one GCFTR-2 can "support" three 1000 MW(electric) LWRs. At the current rate of electricity production by nuclear power facilities in the United States (104 reactors), the national production of TRU could be offset with the deployment of a fleet of 35 GCFTRs. Additional units would allow for the depletion of TRU stockpiles contained within more than 60 000 tonnes of SNF dispersed throughout the country. This depletion of the TRU content of LWR SNF would significantly reduce the repository requirements of a geologic repository and increase the proliferation resistance of that facility.

TABLE XVI

3000-MW(thermal) GCFTR-2 Fuel Cycle Parameters

Parameter	
Fuel/matrix (by volume)	70/30
Total core TRU volume (%)	4.57
Core coolant volume (%)	20.0
Core fuel volume (TRISO + matrix) (%)	59.5
Core cladding volume (%)	10.0
Core Li_2O volume (%)	0.5
Cycles/residence time (batches)	5
Cycle length (days)	600
Once-through residence time (yr)	8.21
Beginning-of-cycle k_{eff}	0.95
End-of-cycle k_{eff}	0.81
Beginning-of-cycle P_{fus} (MW)	38
End-of-cycle P_{fus} (MW)	137
TRU BOC load (tonnes)	51
TRU burned per year (tonnes/FPY)	1.11
TRU burned per cycle (tonnes)	1.8
TRU burned per residence time (tonnes)	9.1
TRU burn/cycle (%)	3.6
TRU burn/residence (%)	16.8
SNF disposed per year (tonnes/FPY)	99.3
Average core flux across cycle (n/cm^2·s)	4.25E+14[a]
Average core (>0.11 MeV) flux (n/cm^2·s)	1.98E+14
Fluence/residence time (n/cm^2)	1.10E+23
Fluence (>0.11 MeV)/residence time (n/cm^2)	5.14E+22
Residence at 90% burn (yr)	103
Fluence at 90% burn (n/cm^2)	1.38E+24
Fluence (>0.11 MeV) at 90% burn (n/cm^2)	6.45E+23
Residence at 99% burn (yr)	205
Fluence at 99% burn (n/cm^2)	2.75E+24
Fluence (>0.11 MeV) at 99% burn (n/cm^2)	1.28E+24

[a]Read as 4.25×10^{14}.

VI. FUSION NEUTRON SOURCE

VI.A. Plasma Physics and Engineering Systems Analysis

Standard tokamak systems analysis methodology[45] was used to determine the major operational and geometric parameters in terms of the aspect ratio (major radius/minor radius) and plasma current, taking into account the various plasma physics and engineering constraints as well as the geometric constraint on the radial build. A reference fusion neutron source was chosen with the nominal parameters for the most part well within the limits of the present plasma physics and fusion technology database, as given in Table XVII. For the sake of comparison, the parameters of the planned ITER experiment,[6] which would serve as a prototype of the GCFTR-2 neutron source, are also given.

VI.B. Superconducting Magnet Dimensions

The superconducting magnet design for the original GCFTR design[5] was adapted directly from the ITER

TABLE XVII

Tokamak D-T Fusion Neutron Source Nominal Parameters

Parameter	GCFTR-2	ITER[a]
Fusion power, P_{fus} [MW(thermal)]	180	410
Neutron source strength (number per second)	7.1×10^{19}	14.4×10^{19}
Major radius, R (m)	3.72	6.2
Minor radius, a (m)	1.08	2.0
Plasma elongation, h/w	1.7	1.8
Plasma current, I (MA)	8.3	15.0
Fusion power/plasma heating power	3.1	10
Magnetic field in plasma, B_φ (T)	5.7	5.3
Confinement factor[b] $H_{IPB98}(y,2)$	1.0	1.0
β_N = (plasma pressure/magnetic pressure)/(I/aB_φ)	2.0[c]	1.8
Bootstrap current fraction, f_{bs}	0.31	
Current drive efficiency, γ_{cd} (A/W·m^2)	0.61[d]	
14-MeV neutron wall flux, Γ_n (MW/m^2)	0.6	0.5
Heat flux to wall, q''_w (MW/m^2)	0.23	0.15

[a]Reference 6.
[b]Enhancement factor relative to present database.
[c]Present database ≤2.5.
[d]Present database ≤0.45.

design.[45,46] This design was based on cable-in-conduit Nb_3Sn conductors operating at magnetic field strengths up to 11.8 T for the toroidal field coils (TFCs) and 13.5 T for the central solenoid. After completion of the GCFTR design, it was realized that the scaling of the TFC design had allowed more space than was actually needed to contain the conductors necessary to produce the required toroidal field, and a preliminary reexamination of the magnet design indicated that the radial thickness of the TFCs could be reduced to 0.43 m. The purpose in this section is to reexamine the radial thickness determinations for the central solenoid and TFCs.

The first step in examining the radial magnet dimensions was a verification of the central solenoid dimensions. Two limiting factors were considered. The tensile stress should be <430 MPa (Ref. 45), and the start-up volt-seconds, VS_{start}, should be above the 82.5 V·s required for inductive start-up.

An approximate equation for the central solenoid stress is as follows[47]:

$$C \cdot \frac{1}{f_{structure}} \cdot \left(\frac{B_{OH}^2}{2 \cdot \mu_0} \right) \left(\frac{R_{fc}}{\Delta_{OH}} + \frac{1}{3} \right) R_{fc}^2 \leq 430 \text{ MPa} \ .$$

Here, the scaling constant $C \approx 1.4$ and the volume fraction of the structural material is $f_{structure} = 0.564$. The magnetic field for the central solenoid is 13.5 T. The flux core radius $R_v = 0.66$ m, and the thickness of the central solenoid coil $\Delta_{OH} = 0.70$ m. Evaluation of the above equation yields ~230 MPa, which is well below the tensile limit of 430 MPa (Ref. 5), confirming that the thickness of the central solenoid coil is adequate to support the electromagnetic force.

The start-up volt-seconds requirement may be written as follows[47]:

$$\pi \cdot \Delta B_{OH} \cdot R_v^2 \left[1 + \frac{\Delta_{OH}}{R_v} + \frac{1}{3} \cdot \left(\frac{\Delta_{OH}}{R_v} \right)^2 \right] \geq \text{VS}_{req\text{-}start} \ ,$$

where $\Delta B_{OH} \approx 2B_{OH}^{\max} = 26.3$ T. Evaluation of this expression yields 87.7 V·s, satisfying the start-up requirement of $\text{VS} \geq \text{VS}_{startup\text{-}required} = 82.5$ V·s and confirming $R_v = 0.66$ m.

The second part of the magnet analysis involved the TFCs, for which the preliminary estimate of 0.43 m for the radial width was confirmed by scaling down the ITER TFC dimensions by conserving the ITER tensile stress ≈ magnetic force/structural cross-sectional area. This magnetic force is roughly equal to a constant times the square of the current in each toroidal field leg so that the stress is $\sigma = F/A = (CI^2)/A$. Here, A equals the cross-sectional area of the structural material in each TFC. In GCFTR-2 the required current in each coil is 6.4 MA. In ITER (Ref. 6) $I = 9.13$ MA and $A = 0.3$ m^2. This scaling then leads to the area for GCFTR-2, $A = 0.15$ m^2, which works out to a radial thickness $\Delta_{TF} = 0.43$ m. It was then confirmed that the required number of conducting strands can fit in this geometry. Note that this scaling procedure does not take into account local stresses due to support structures, etc., analysis of which would require methods beyond the scope of this study.

In summary, the superconducting magnet system design of GCFTR (Ref. 5) was adopted for GCFTR-2, with the single exception of reducing the radial thickness of the TFCs to 0.43 m. The flux core radius of 0.66 m, the central solenoid radial thickness of 0.70 m, the cable-in-conduit conductor design, the total current, and the maximum field capability remain unchanged.

VI.C. Tritium Production

The objective of using current reactor technologies or near-term technologies with respect to tritium self-sufficiency was achieved by placing He-cooled Li_2O tritium breeding elements (TBEs) in both the outboard and inboard blanket shields, as well as replacing 0.2% (by volume) of the fuel pins in the reactor core with Li_2O pins.

The TBE design consists of a wall made of structural materials with ceramic breeder pebbles inside. Several designs have been proposed for such breeding blanket concepts,[48] which were modified to fit within the blanket and shield regions of the GCFTR-2. The TBE will be cooled by high-pressure helium flowing through tubes in the core. The tritium will be swept out of the blanket into a separate helium purge gas flow and removed online into a tritium processing system. In order to meet tritium self-sufficiency requirements, Li_2O pins also must be placed inside the transmutation reactor core with their own He purge gas system.

The tritium breeding material will be lithium oxide (Li_2O) enriched in ^{6}Li. Li_2O was selected because of its higher atomic density of lithium as opposed to other potential ceramics (Li_2TiO_3, Li_2ZrO_3, etc.). Drawbacks of this choice are that Li_2O is hydroscopic and exhibits poor chemical stability. Additionally, the temperature window for operation is smaller than that of the alternatives. The Li_2O operating temperature range is ~400 to 800°C (Ref. 48). Below this temperature the pebbles are unable to release the tritium, because the diffusivity of the tritium to the surface of the microparticles becomes too small. Above this temperature range, the swelling of the particles increases and closes off the porosity, thus preventing the migration of the tritium into the purge gas stream. Optimal operating temperature would be closer to the lower limit of the range.[48] Li_2O has a melting point of 1570°C.

The tritium production design will consist of 90% enriched natural lithium in the outboard blanket shield in order to take advantage of the large ^{6}Li cross section in the thermal neutron energy range. The inboard reflector region will be enriched to only 30% ^{6}Li because tritium production from the ^{7}Li reaction is more prevalent in the higher energy neutron flux emerging inward from the

fusion plasma source. The Li_2O microparticles are considered to be at 90% theoretical density (the theoretical density of Li_2O is 2.013 g/cm^3). A beryllium neutron multiplier will be employed in the TBE. The dimensions and materials of the TBEs are described in Sec. IV.

The net production of tritium must exceed the net losses of tritium through burnup in the plasma by a margin adequate enough to compensate for losses and the radioactive decay during extraction and storage between production and use. Some loss of tritium can also be attributed to the fractional buildup between 0.01 and 0.5, which is inversely proportional to the flow rate into the plasma.[49] The models used to calculate tritium self-sufficiency depend on rather uncertain estimations of losses and error. Studies show an uncertainty of roughly 5 to 7% is to be expected.[50]

To be certain that self-sufficiency is attained, a number greater than the theoretical requirement is necessary. Using the analysis of Ref. 49, it is estimated that a minimum tritium breeding ratio of >1.06 is required to achieve tritium self-sufficiency of the GCFTR-2. Allowing for reasonable uncertainties (5%) and using the parameters in Table XVIII, the estimation is required TBR ≈ 1.12.

The required (Λ_r) and achievable (Λ_a) ratios were calculated from the following[8]:

$$\Lambda_r = 1 + G_0 + \Lambda_G$$

and

$$\Lambda_a = \Lambda_c - \sqrt{\Delta_S^2 + \Delta_P^2} \ ,$$

where

G_0 = tritium breeding margin to compensate for holdup, losses, decay, and reserves

Δ_G = uncertainties in breeding margin in reference parameters

Λ_c = calculated TBR

Δ_S^2 = uncertainties in system definition

Δ_P^2 = uncertainties in predicting TBR due to uncertainties in nuclear data, calculation methods, and geometrical representation.

It is estimated that a beginning of cycle inventory of 144 g will be required.[47] The inventory will need to be sufficient to cover tritium consumption at a higher fusion power than the nominal upper limit of 180 MW, if that should prove to be necessary. The maximum tritium inventory is estimated to be ~1.2 kg (Ref. 47).

TABLE XVIII

Parameters for Tritium Losses*

Parameter	Value	Definition
ε_2	0.001	Breeder processing loss
ε_3	0.001	Blanket coolant processing loss
ε_4	0	Fuel cleanup and isotope separation unit loss
ε_6	0.001	Plasma exhaust processing loss
ε_7	0.001	Limiter coolant processing loss
ε_8	0.001	First-wall coolant processing loss
β	0.05	Tritium fractional burnup in plasma
f_c	0.01	Breeder-to-blanket leakage
f_L	0.0001	Plasma-to-limiter leakage
f_F	0.0001	Plasma–to–first-wall leakage

*Reference 48.

VI.D. Divertor and First Wall

The divertor and first-wall design for the fusion neutron source were adapted for He cooling from the ITER design,[6] which uses water flowing through channels located in the structure for cooling. A detailed drawing of the ITER divertor was scaled down (Fig. 13) to serve as the model for the heat removal calculations described in Sec. VII. The model was scaled down such that the width of the divertor would reach approximately halfway out in the plasma region. The divertor targets are lined with tungsten tiles backed with a layer of copper that bonds the tiles to CuCrZr alloy matrix. Cooling fins must be added behind the targets to achieve adequate heat removal with He cooling. The first wall consists of a 2-cm-thick plate of ferritic steel (e.g., HT-9) coated on the plasma-facing side with 0.5 cm of Be and cooled by He.

VII. THERMAL DESIGN

VII.A. Core Thermal Design

To support the selection between the pin and block fuel element options discussed in Sec. III, thermal analyses were performed for each type under steady-state conditions.

VII.A.1. Steady-State Analysis: Fuel Pins

The reactor fuel design was based upon a standard PWR pin, that is, fuel material surrounded by an inert gas "gap" blanket and a cladding structure. Two pin types were considered, one composed of BISO fuel pellets suspended within a zirconium carbide matrix and the other composed of TRISO fuel pellets suspended within a silicon carbide matrix. The dimensions of the fuel pin are provided in Table XIX and Fig. 5.

At 3000 MW(thermal) uniformly distributed power in the reactor, the average volumetric fission heat source is $q''' = 42.2$ MW/m^3, which was used in the thermal analysis. With a He mass flow rate of 2870 kg/s, the He coolant entered at 280°C and exited at 494°C, and the core He pumping power was 0.15 MW.

TABLE XIX

Fuel Pin Dimensions

Fuel Outer Radius	Clad Inner Radius	Clad Outer Radius
0.60 cm	0.61 cm	0.67 cm

The temperature distribution in a fuel pin was evaluated at three different axial locations in an average coolant channel in the core: the inlet, the outlet, and the arithmetic mean "bulk" temperature. In order to apply a thermal resistance model, the fuel pin must be treated as a homogeneous mixture of the fuel kernels, matrix, gas gap, and Zircaloy cladding. The thermal conductivities for the various pin components are listed in Table XX.

The heat transfer coefficient (h) for the helium coolant was dependent upon the coolant channel geometry and helium flow conditions and was calculated[52] to be 4161.81 W/m^2·°C.

The homogenized thermal conductivities for the two pin loadings were based upon the volume fraction for each pin type. The homogenized conductivities for the BISO/ZrC and TRISO/SiC pins were 16.87 and 51.76 W/m·°C, respectively. Application of the thermal resistance model resulted in the distribution plotted for the TRISO/SiC pins in Fig. 14. Similar temperature distributions were found for the BISO/ZrC pins. Heat removal from both fuel types thus is readily accomplished under nominal steady-state operating conditions since the lowest melting temperature among the pin components is that of the Zircaloy cladding at 1845°C.

Figure 14 is based on a uniform core power distribution and nominal values of heat conductivities and fuel dimensions. Radiation damage can produce a degradation of thermal conductivity in SiC and a swelling of the Zircaloy cladding (which has the effect of reducing the coolant flow area). Furthermore, power peaking introduced by fuel burnup and shuffling can increase the heat source in limiting pins. We have allowed a factor of ~3.5 to clad melting to compensate for these details, the evaluation of which are beyond the scope of this initial study.

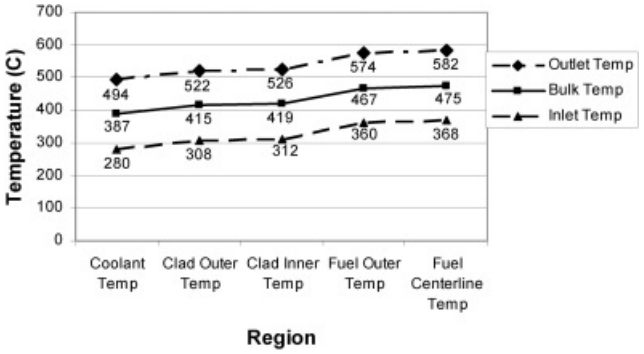

Fig. 14. TRISO/SiC pin temperature distributions (inlet, outlet, and midway).

VII.A.2. Fluent Calculation: Fuel Pins

The steady-state condition of the fuel pins under normal load also was investigated by modeling one pin centered in a hexagonal box of helium coolant that represents a unit cell for one pin. The following programs were used: A 3-D computer-aided design program called Solid Edge[53] was used to build a fuel pin that had a radius of 0.67 cm and a height of 3 m and the equivalent cell, GAMBIT[54] was used to mesh nodes in the rod and cell, and a computational fluid dynamics program called Fluent[54] was used to model the steady-state temperature distribution in the pin and the coolant, using the parameters in Table XXI. This resulted in a somewhat smaller peak centerline temperature of 535°C at the top of the core but the same outlet coolant temperature of 494°C. The average coolant velocity was ~85 m/s.

VII.A.3. Steady-State Analysis: LDGF

A thermal analysis, using the thermal resistance model,[55] of the LDGF in a hexagonal fuel matrix (see

TABLE XX

Fuel Pin Component Heat Conductivities*

Pin Component	Thermal Conductivity (W/m·°C)
Silicon carbide matrix[a]	120
Zirconium carbide matrix	18.94
BISO fuel	15.18
TRISO fuel	6.49
Helium gap	0.26
Zircaloy cladding	18.94
Helium heat transfer coefficient	4161.81 W/m^2·°C

*Reference 5.
[a]Reference 51.

TABLE XXI

Fluent Model Parameters

He mass flow rate	0.01435 kg/s·cell
Volumetric heat generation of rod	42.17 MW/m^3
He inlet temperature	280°C
Turbulence model	k-ε RNG method
Inlet turbulence	5%
He inlet pressure	7 MPa
$k_{homogenized\ rod}$	51.759 W/m·K
k_{helium}	0.26 W/m·K
He viscosity	3.37×10^{-5} kg/m·s

Fig. 6) was performed. The only calculation that was performed for LDGF steady-state analysis was the bulk temperature at the midplane of the core. When calculating the bulk LDGF temperature, the following assumptions were made: The same coolant pumping power, mass flow rate, power density, and volume percentage of coolant were used as in the above pin calculation. The thermal properties of the LDGF and the fuel configuration were different, of course. The maximum bulk midplane temperature in the LDGF fuel block was determined to be 484°C (TRISO) and 483°C (BISO) at the edges of a typical block within the core (Fig. 15), which is slightly more than the midplane centerline fuel pin temperature of 475°C. Thus, there is essentially no difference in the nominal steady-state heat removal properties of the fuel pin and fuel block configurations.

VII.B. LOCA

A complete loss of the flow of coolant was considered. Predicting the consequences of such an accident is necessary in order to know whether or not passive safety is possible. When such an accident occurs, it is assumed that the neutron source is immediately shut down and there is no more heat produced by fission. However, there is still heat generated as decay heat from (primarily) fission products. This decay heat calculated using the ORIGEN-S (Ref. 31) code is shown in Fig. 16 for fuel irradiation periods of 5, 0.5, and 0.1 yr in GCFTR-2. The decay heat from typical PWR fuel is shown for comparison.

When the flow of coolant is completely stopped in a LOCA, the only significant form of heat transfer that would remove the decay heat from the fuel pins is radiation. There also would be a slight amount of conduction through structural material, but that form of heat transfer was ignored because of its insignificance. A MATLAB code was written in order to calculate the temperature change in the pins during a LOCA.

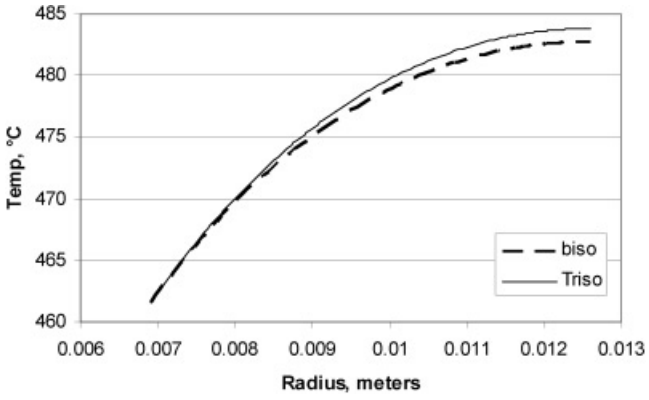

Fig. 15. Steady-state temperature distribution of an average hexagonal graphite assembly.

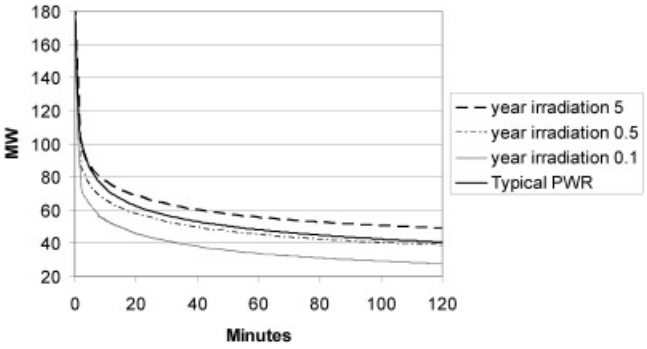

Fig. 16. Decay heat.

To calculate the heat lost from radiation, view factors for the fuel pin configuration needed to be obtained. For a horizontal cross section of the core, each interior fuel pin is surrounded by six pins, and there are six channels between adjacent pins where heat can escape (see Fig. 5). Using the reference pin pitch and diameter given above, the view factor for each adjacent pin is ~0.157. This means that ~15.7% of the heat that can be emitted by radiation from one pin is incident directly on each of the six adjacent pins. Similarly, a view factor of ~1% was obtained from a pin to the channel between two adjacent pins. Exterior pins in the assembly had a view factor to the assembly wall of 34.4%. Thus, the exterior pins would radiatively cool first by radiating to the assembly wall, the second row of pins would cool by radiating to the exterior pins, etc. Heat is also radiated out vertically from the tops and bottoms of the fuel pins, and the vertical view factor for these surfaces to the walls of the core was assumed to be 100%.

At the beginning of the LOCA, it was assumed that the temperature of each pin was 408°C. It was assumed that the pins and the reactor walls were blackbodies and no heat was reflected from the surface. The MATLAB code calculated the amount of heat generated in each radial row of fuel pins for each minute and then calculated the temperature change due to that heat addition. These temperature differences were important in calculating the amount of heat that would radiate away from the pins, because in order for a net amount of heat to be radiated away from a pin, the surrounding surfaces must be at a lower temperature than the pin itself. The heat was then added to adjacent rows of pins or the reactor walls and then new temperatures were calculated. This calculation was carried out for the first 48 h after a LOCA occurs.

It was determined by this calculation that under radiation heat removal only, the Zircaloy cladding on the fuel pins would melt (1845°C) at ~25 min after the LOCA starts, and the TRU fuel kernel would melt (2035°C) a few minutes later, as shown in Fig. 17. Thus, the reactor is not passively safe and must be designed with an active

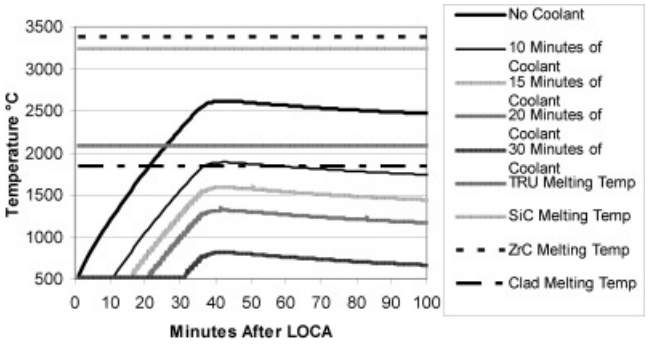

Fig. 17. Fuel temperature during LOCA with and without emergency core cooling.

safety system in order to prevent melting of the clad and TRU kernel in a LOCA. However, after ~50 min the decay heat that would be generated would be able to be removed by radiation without the melting temperature of any part of the fuel being exceeded. Therefore, an active safety system would need to supply emergency coolant only within the initial hour of a LOCA.

The calculations were repeated with emergency helium injection for varying durations during a LOCA, using the decay heat source that would be present after 5 yr of fuel burnup. The emergency cooling system was assumed to operate in a fashion similar to that of the primary cooling system; that is, the heat transfer coefficient h was assumed to be the same. In addition, the fuel pin temperature was assumed to remain at steady-state levels for the duration of emergency cooling, although under actual conditions the pin temperature would decrease. This assumption was made so as to add a degree of conservatism to the calculation.

Figure 17 shows the fuel pin temperature as a function of time under a LOCA scenario as related to several melting temperatures, the lowest one being that of the cladding at 1845°C. If there is no emergency coolant injection, the Zircaloy cladding (1845°C melting point) and the TRU kernel (2035°C melting point) would both melt, but the ZrC (3250°C melting point) and SiC (3375°C melting point) would not. For the entire core to survive a LOCA without any fuel melting, a minimum of 10 to 15 min of emergency helium cooling (1.7 to 2.6×10^6 kg) would be required. Potential brittle fracture problems could be encountered if this is stored in the liquidized state.

If the pins were designed without the Zircaloy cladding, the only material to melt during the LOCA would be the TRU kernel. Since the kernel is encased in ZrC and pyrolytic graphite coatings, which would not melt, it might be argued that the design would be passively safe if the Zircaloy cladding could be omitted.

VII.C. Divertor Heat Removal

Although the divertor design was adapted from the ITER H_2O-cooled design (Fig. 13), heat removal from the GCFTR-2 He-cooled divertor differs significantly because of the choice of coolant. Some form of fins will be needed in the void space behind the vertical targets in order to adequately remove the heat from the structure. The calculations to determine the amount of divertor heat removal were made with Fluent[54] by using a highly simplified 3-D model made in Solid Edge[53] and meshed in GAMBIT (Ref. 54). The Fluent model uses a large void space behind the tiles with no cooling fins and a divertor depth of 1 m. From this a steady-state temperature distribution for the modified ITER design, which is now helium cooled instead of water cooled (no cooling fins), was found for two surface heat fluxes, 1 and 2 MW/m^2. This information determines the additional heat removal requirement for a set of fins that would be able to remove enough heat to obtain an acceptable temperature distribution.

The entire structure is modeled as CuCrZr that has a density of 8900 kg/m^3, specific heat of 376 $J/kg \cdot K$, and thermal conductivity 320 $W/m \cdot K$. The required helium mass flow rates for the 1 and 2 MW/m^2 cases are 77.1 and 231.2 kg/s, respectively, and the inlet pressure is 7 MPa. The pumping power for the helium through the divertor was calculated[5] to be 143.6 MW. The turbulence is modeled the same way as described above for the equivalent unit cell for the fuel pins, except that a 10% turbulence intensity was set for the inlet. The temperature of the plasma-facing components has a surface profile that starts out cool and gradually becomes hotter at the outlet. The maximum temperature seen is 1217°C for the 1 MW/m^2 case and 1417°C for the 2 MW/m^2 case.

Knowing the mass and the maximum temperature of the plasma-facing component, a calculation was performed using the specific heat of the material to determine how much energy needs to be removed to lower the temperature to a safe level. For the sake of the study, 1000°C was defined as a safe temperature. For the 1 and 2 MW/m^2 cases, 74 and 142 MJ, respectively, need to be removed from the steady-state condition to lower the temperature to 1000°C. An appropriate fin design that would remove energy at this rate would allow safe operation of the GCFTR-2 divertor.

VII.D. Secondary System and Electrical Performance

A secondary electrical system is needed to convert the heat to useful electrical work. Since helium is the coolant for the reactor, a typical Brayton cycle[56] will be used, which utilizes the He directly. In order to realistically utilize the 3000 MW(thermal) that is being produced in the core, a total of four Brayton cycles will be used, one for each 90-deg segment of the reactor. Therefore, each Brayton cycle corresponds to 750 MW(thermal). Figure 18 shows one of the Brayton cycles, and Table XXII identifies the properties at each section of the thermodynamic cycle.

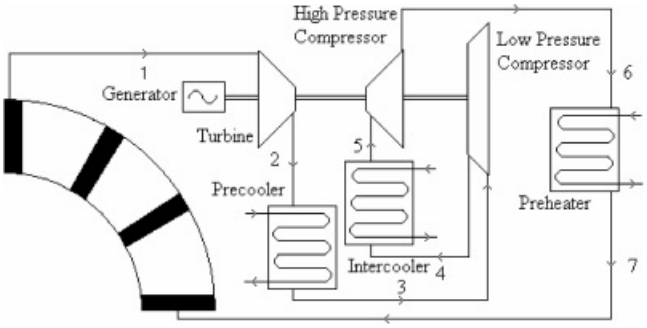

Fig. 18. Secondary electrical system diagram (Brayton cycle).

The total electrical power that is extracted from the 750-MW cycle is 255 MW(electric), corresponding to a thermal efficiency of 34%. The total electrical power for the entire reactor is 1020 MW(electric). However, to calculate the net amount of electrical power, the operating power requirements must be taken into consideration. These losses include power for all of the magnets involved in confinement (~30 MW), the heating and current-drive systems for the plasma [90 MW (Ref. 5)], and the coolant pumping power for both the core and the divertor (~200 MW). After taking into account all of the power used to operate the reactor, the net electrical power for the entire system is 700 MW(electric). The electrical power amplification factor (Q_e) is calculated as the total electrical power divided by the net operating power requirements, and this equals 3.19.

VIII. SUMMARY

A design concept for a subcritical GCFTR driven by a tokamak D-T fusion neutron source has been analyzed and further evolved. The GCFTR-2 objectives are (a) to obtain deep burn (>90%) of TRU extracted from SNF by utilizing coated fuel particle (TRISO or BISO) technology and (b) to base the design on near-term physics and technologies that are being developed in the U.S. Department of Energy nuclear and fusion programs and corresponding international programs.

We considered coated TRU fuel embedded in SiC or Zircaloy to form fuel pins or embedded in LDGF to form solid fuel blocks, all He-cooled, as fuel options. All options had similar heat removal characteristics under nominal steady-state conditions and under LOCA conditions. The TRISO/SiC fuel pin option resulted in the largest ratio of transmutation rate to neutron damage rate and the most negative or least positive coefficients of reactivity. The graphite foam fuel block option was rejected because of excessive brittleness and a high-temperature step in the formation process that exceeded the melting temperature of the TRU kernel in the coated fuel particle. The TRISO/SiC fuel pin option was chosen over the BISO/Zircaloy fuel pin option because of superior neutronics properties for transmutation.

The annular fast transmutation reactor core (R_{in} = 485 cm, W = 112 cm, H = 300 cm) will be 59.8 vol% fuel, 0.2 vol%, Li_2O, 30 vol% He, and 10 vol% structure; the fuel will be 62.8 vol% coated TRU particles and 37.2 vol% SiC. The core would operate at $k_{eff} \leq 0.95$, P_{th} = 3000 MW(thermal) at a nominal power density of 42 MW/m^3 and a tritium breeding ratio ≥1.1 to achieve tritium self-sufficiency. The He mass flow rate of 2870 kg/s at T_{in} = 280°C and T_{out} = 494°C would limit the maximum fuel temperature to 582°C under normal operation. For the entire core to survive a LOCA without any Zircaloy clad melting, a minimum of 10 to 15 min of emergency helium cooling would be required during the first hour.

The subcritical reactor would be driven by a superconducting tokamak D-T fusion neutron source that would produce up to 180 MW of power and a neutron source rate of 6.5×10^{19}/s. The major parameters of the tokamak plasma are (R_{major} = 3.73 m, $\beta_N \leq 2.0$, $Q_p \approx 3$, H_{98} = 1). The plasma physics and fusion technology design basis for the neutron source is the same as for ITER, except for modest extensions in current-drive efficiency, and ITER operation would serve as a prototype.

At a thermal power of 3000 MW/FPY, the GCFTR-2 transmutes ~1.11 tonnes of TRUs, which is equivalent to the TRU production rate of three 1000-MW(electric) LWRs per FPY. The GCFTR-2 produces 700 MW net electrical power and operates with an electrical multiplication factor Q_e = 3.2.

TABLE XXII

Thermodynamic Properties of Brayton Cycle

Section	Temperature (°C)	Pressure (MPa)
1	494	7.00
2	122	2.41
3	25	2.41
4	66	3.09
5	25	3.09
6	151	7.00
7	300	7.00

REFERENCES

1. "GEN-IV International Forum: Nuclear Energy Systems for the Future," available on the Internet at http://www.gif.inel.gov/.

2. "Advanced Fuel Cycle Initiative," available on the Internet at http://www.nuclear.gov/afci.

3. F. H. SOUTHWORTH et al., "The Next Generation Nuclear Plant (NGNP) Project," *Proc. Global 03*, New Orleans, Louisiana, November 16–20, 2003, American Nuclear Society (2003) (CD-ROM).

4. C. RODRIGUEZ et al., "Deep-Burn: Making Nuclear Waste Transmutation Practical," *Nucl. Eng. Des.*, 2805 (2003).

5. W. M. STACEY et al., "A Subcritical, Gas-Cooled Fast Transmutation Reactor with a Fusion Neutron Source," *Nucl. Technol.*, **150**, 162 (2005).

6. International Tokamak Experimental Reactor; available on the Internet at http://www.iter.org; also "ITER Detailed Design Report, Cost Review and Safety Analysis," International Thermonuclear Reactor Project (1996); also "The ITER Project L-7 Implementation," ENEA; available on the Internet at www.brasimone.enea.it/iterl-7 (1998).

7. E. LONG et al., "Fabrication of ORNL Fuel Irradiated in the Peachbottom Reactor and Post-Irradiation Examination of the Recycle Test Elements 7 and 4," Oak Ridge National Laboratory (Oct. 1974).

8. D. A. PETTI et al., "Key Differences in the Fabrication, Irradiation and High Temperature Accident Testing of U.S. and German TRISO-Coated Particle Fuel, and Their Implications on Fuel Performance," *Nucl. Eng. Des.*, **222**, 281 (2003).

9. B. B. KADOMTSEV et al., "USSR Contribution to the Phase IIA INTOR Workshop," Vol. 2, p. VIII-64 (1982).

10. M. SAWAN, University of Wisconsin, Personal Communication (2004).

11. M. KUBOTA, Y. MORITA, I. YAMAGUCHI, I. YAMAGISHI, T. FUJIWARA, and M. WATANABE, "Development of the Four Group Partitioning Process at JAERI," *Fifth OECD/NEA Information Exchange Meeting on Actinide and Fission Product Partitioning and Transmutation*, Session 2, pp. 1–9 (1998).

12. M. C. THOMPSON, M. A. NORATO, G. F. KESSINGER, R. A. PIERCE, T. S. RUDISILL, and J. D. JOHNSON, "Demonstration of the UREX Solvent Extraction Process with Dresden Reactor Fuel Solution," Westinghouse Savannah River Company (2002).

13. "Implications of Partitioning and Transmutation in Radioactive Waste Management," International Atomic Energy Agency (2003).

14. C. MADIC, "Overview of the Hydrometallurgical and Pyro-Metallurgical Processes Studied Worldwide for the Partitioning of High Active Nuclear Wastes," *OECD/NEA 6th Information Exchange Meeting*, Madrid, Spain, pp. 53–64, Organization for Economic Cooperation and Development/Nuclear Energy Agency (2000).

15. E. ZIMMER and C. GANGULY, "Reprocessing and Refabrication of Thorium-Based Fuels," Institut für chemische Technologie der nuklearen Entsorgung, Kernforschungsanlage Jülich GmbH; available on the Internet at http://www.iaea.org/inis/aws/fnss/fulltext/0412_8.pdf (2005).

16. J. J. LAIDLER, L. BURRIS, E. D. COLLINS, J. DUGUID, R. N. HENRY, J. HILL, E. J. KARELL, S. M. McDEAVITT, M. THOMPSON, M. A. WILLIAMSON, and J. L. WILLIT, "Chemical Partitioning Technologies for an ATW System," *Prog. Nucl. Energy*, **38**, *1–2*, 65 (2001).

17. D. E. CLARK, J. B. WHITE, and A. J. MACHIELS, "Nuclear Waste Management," *Advances in Ceramics*, Vol. 20, American Ceramic Society, Waterville, Ohio (1986).

18. Reactor Institute Delft; available on the Internet at http://www.iri.tudelft.nl/~rfwww/images/triso.jpg.

19. F. J. HOMAN, T. B. LINDEMER, E. L. LONG, Jr., T. N. TIEGS, and R. L. BEATTY, "Stoichiometric Effects on Performance of High-Temperature Gas-Cooled Reactor Fuels from the U-C-O System," *Nucl. Technol.*, **35**, 428 (1977).

20. T. B. LINDEMER, "Thermochemical Analysis of Gas-Cooled Reactor Fuels Containing Am and Pu Oxides," ORNL/TM-2002/133, Oak Ridge National Laboratory (2002).

21. H. HAYASHI, K. SAWA, and Y. KOMORIL, "Irradiation Experiences and the Future Plan in the HTTR Project," *Proc. Int. Symp. Research Reactor and Neutron Science*, Daejeon, Korea, April 25–29, 2005, Korean Atomic Energy Research Institute (2005).

22. W. CORWIN and J. KLETT, "High Conductivity Graphite Foams and Applications," Oak Ridge National Laboratory (May 2004).

23. R. A. KARAM et al., "High Temperature Gas-Cooled Fast Reactor," *Proc. Int. Conf. Advanced Power Plants*, Seoul, May 14–20, 2005.

24. W. J. LACKEY and T. L. STARR, "Fabrication of Fiber Reinforced Ceramic Composites by Chemical Vapor Infiltration: Processing, Structure and Properties," *Fiber Reinforced Ceramic Composites*, K. S. MAZDIYASNI, Ed., Noyes Publications, Park Ridge, New Jersey (1990).

25. J. KLETT, Oak Ridge National Laboratory, Private Communication (2005).

26. J. F. SHACKELFORD and W. ALEXANDER, Eds. *CRC Materials Science and Engineering Handbook*, CRC Press, Boca Raton, Florida (2000).

27. T. BESMANN, "Chemical Vapor Infiltration Modeling and Processing of Energy-Related Materials," Oak Ridge National Laboratory (Nov. 1999).

28. K. MINATO and T. OGAWA, "Research and Development of ZrC Coated Particle Fuel," *Proc. Atoms for Prosperity (Global 03)*, p. 1068, American Nuclear Society (2003) (CD-ROM).

29. C. T. WALKER, T. KAMEYAMA, S. KITAIMA, and M. KINISHITA, "Concerning the Microstructure Changes that Occur at the Surface of UO_2 Pellets on Irradiation to High Burnup," *J. Nucl. Mater.*, **188**, 73 (1992).

30. H. BAILLEY, D. MENESSIER, and C. PRUNIER, *The Nuclear Fuel of Pressurized Water Reactors and Fast Reactors:*

Design and Behaviour, Chap. 5, p. 427, Intercept Ltd, Hampshire, United Kingdom (1999).

31. "ORIGEN-S: SCALE System Module to Calculate Fuel Depletion, Actinide Transmutation, Fission Product Buildup and Decay, and Associated Radiation Source Terms," NUREG/CR-200, Revision 7 (ORNL/NUREG/CSD-2/V2/R7), Oak Ridge National Laboratory (2004).

32. T. SALING, *Radioactive Waste Management*, Hemisphere Publishing Corporation, New York (1990).

33. R. RASMUSSEN, "Dry Storage Option for Spent Fuel Management," *Proc. USCEA Fuel Cycle Conf.*, New Orleans, Louisiana (1988).

34. R. COCHRAN and N. TSOULFANIDIS, *The Nuclear Fuel Cycle: Analysis and Management*, American Nuclear Society, La Grange Park, Illinois (1990).

35. Information available on the Internet at www.wisconsinmetaltech.com.

36. C. DE OLIVEIRA and A. GODDARD, "EVENT—A Multidimensional Finite Element-Spherical Harmonics Radiation Transport Code," *Proc. Int. Seminar 3-D Deterministic Radiation Transport Codes*, Paris, France, Organization for Economic Cooperation and Development (1996).

37. H. HENRYSON et al., "MC^2-2: A Code to Calculate Fast Neutron Spectra and Multigroup Cross Sections," ANL-8144, Argonne National Laboratory (1976).

38. "DANTSYS: A Diffusion Accelerated Neutral Particle Transport Code System," LA-12969-M Manual UC-705, Los Alamos National Laboratory (1997).

39. J. F. BRIESMEISTER, Ed., "MCNP—A General Monte Carlo *N*-Particle Transport Code," Version 4B, LA-12625-M, Los Alamos National Laboratory (1997).

40. I. C. GAULD, O. W. HERMANN, and R. M. WESTFALL, NUREG/CR-0200, 7th ed., Vol. 2, Chap. 3, p. 99 (2004).

41. "Understanding NJOY," LA-UR-00-1538, Los Alamos National Laboratory; available on the Internet at http://t2.lanl.gov/njoy/ (2000).

42. B. J. TOPPEL, "A User's Guide to the REBUS-3 Fuel Cycle Analysis Capability," ANL-83-2, Argonne National Laboratory (1983).

43. "KENO V.a: An Improved Monte Carlo Criticality Program," NUREG/CR-0200, Revision 7, Vol. II, Sec. F11, ORNL/NUREG/CSD-2/R7, Oak Ridge National Laboratory (2004).

44. J. D. GALAMBOS et al., "Commercial Tokamak Reactor Potential with Advanced Tokamak Operation," *Nucl. Fusion*, **35**, 551 (1995).

45. M. HUGUET, "Key Engineering Features of the ITER-FEAT Magnet System and Implications for the R&D Programme," *Nucl. Fusion*, **41**, 645 (2001).

46. ITER Technical Basis, Chap. 2.1, "Magnets," G A0 FDR 1 01-07-13 R1.0 (2001).

47. W. M. STACEY et al., "A Fusion Transmutation of Waste Reactor," *Fusion Sci. Technol.*, **41**, 116 (2002).

48. M. A. ABDOU, M. TILLACK, and R. A. RAFFRAY, "Thermal, Fluid Flow, and Tritium Release Problems in Fusion Blankets," *Fusion Technol.*, **18**, 165 (1990).

49. M. A. ABDOU et al., "Deuterium-Tritium Fuel Self-Sufficiency in Fusion Reactors," *Fusion Technol.*, **9**, 250 (1986).

50. M. A. ABDOU et al., "Evaluation of the Prediction Uncertainty in Tritium Production Based on Results from Experiments on an Li_2O Annular Blanket Surrounding a 14 MeV Simulated Line Source," *Fusion Eng. Des.*, **28**, 673 (1995).

51. "Materials/Silicon Carbide (SiC) Properties," 2002. Accuratus; available on the Internet at http://www.accuratus.com/silcar.html (Mar. 2005).

52. M. S. KAZIMI and N. E. TODREAS, *Nuclear Systems I: Thermal Hydraulics Fundamentals*, pp. 16–17, 417, 684–685, Hemisphere Publishing Corporation, New York (1990).

53. "Computer Aided Drawing Solid," Solid Edge, Version 15.0, Solid Works Inc. (2003).

54. "Computational Fluid Dynamics," Fluent/GAMBIT, Version 6.1.22/s.1.2, Fluent Inc. (2004).

55. F. P. INCROPERA and D. P. DeWITT, *Fundamental of Heat and Mass Transfer*, 5th ed., Chap. 3, John Wiley and Sons, New York (2002).

56. M. J. MORAN and H. N. SHAPIRO. *Fundamentals of Engineering Thermodynamics*, 4th ed., pp. 441–467, John Wiley and Sons, New York (2000).